RESEARCH ARTICLE

Identification of *Pik3ca* Mutation as a Genetic Driver of Prostate Cancer That Cooperates with *Pten* Loss to Accelerate Progression and Castration-Resistant Growth

Helen B. Pearson[1,2,3], Jason Li[1,2], Valerie S. Meniel[3], Christina M. Fennell[1], Paul Waring[4], Karen G. Montgomery[1], Richard J. Rebello[1,5], Arthi A. Macpherson[6], Sarah Koushyar[3], Luc Furic[1,2,5], Carleen Cullinane[1,2], Richard W. Clarkson[3], Matthew J. Smalley[3], Kaylene J. Simpson[2,6], Toby J. Phesse[3], Peter R. Shepherd[7,8], Patrick O. Humbert[1,2,4,9,10], Owen J. Sansom[11,12], and Wayne A. Phillips[1,2,13,14]

ABSTRACT

Genetic alterations that potentiate PI3K signaling are frequent in prostate cancer, yet how different genetic drivers of the PI3K cascade contribute to prostate cancer is unclear. Here, we report *PIK3CA* mutation/amplification correlates with poor survival of patients with prostate cancer. To interrogate the requirement of different PI3K genetic drivers in prostate cancer, we employed a genetic approach to mutate *Pik3ca* in mouse prostate epithelium. We show *Pik3ca*^{H1047R} mutation causes p110α-dependent invasive prostate carcinoma *in vivo*. Furthermore, we report that *PIK3CA* mutation and *PTEN* loss coexist in patients with prostate cancer and can cooperate *in vivo* to accelerate disease progression via AKT–mTORC1/2 hyperactivation. Contrasting single mutants that slowly acquire castration-resistant prostate cancer (CRPC), concomitant *Pik3ca* mutation and *Pten* loss caused *de novo* CRPC. Thus, *Pik3ca* mutation and *Pten* deletion are not functionally redundant. Our findings indicate that *PIK3CA* mutation is an attractive prognostic indicator for prostate cancer that may cooperate with *PTEN* loss to facilitate CRPC in patients.

SIGNIFICANCE: We show *PIK3CA* mutation correlates with poor prostate cancer prognosis and causes prostate cancer in mice. Moreover, *PIK3CA* mutation and *PTEN* loss coexist in prostate cancer and can cooperate *in vivo* to accelerate tumorigenesis and facilitate CRPC. Delineating this synergistic relationship may present new therapeutic/prognostic approaches to overcome castration/PI3K–AKT–mTORC1/2 inhibitor resistance. *Cancer Discov; 8(6); 764–79. ©2018 AACR.*

See related commentary by Triscott and Rubin, p. 682.

[1]Peter MacCallum Cancer Centre, Melbourne, Victoria, Australia. [2]The Sir Peter MacCallum Department of Oncology, the University of Melbourne, Parkville, Victoria, Australia. [3]European Cancer Stem Cell Research Institute, Haydn Ellis Building, Cardiff University, Cardiff, United Kingdom. [4]Department of Pathology, the University of Melbourne, Parkville, Victoria, Australia. [5]Cancer Program, Biomedicine Discovery Institute and Department of Anatomy and Developmental Biology, Monash University, Clayton, Victoria, Australia. [6]Victorian Centre for Functional Genomics, ACRF RPPA Platform, Peter MacCallum Cancer Centre, Melbourne, Victoria, Australia. [7]Maurice Wilkins Centre for Molecular Biodiscovery, the University of Auckland, Auckland, New Zealand. [8]Department of Molecular Medicine and Pathology, the University of Auckland, Auckland, New Zealand. [9]Department of Biochemistry and Genetics, La Trobe Institute for Molecular Science, La Trobe University, Bundoora, Victoria, Australia. [10]Department of Biochemistry and Molecular Biology, the University of Melbourne, Parkville, Victoria, Australia. [11]CRUK Beatson Institute, Garscube Estate, Glasgow, United Kingdom. [12]Institute of Cancer Sciences, University of Glasgow, Garscube Estate, Glasgow, United Kingdom. [13]Department of Surgery (St. Vincent's Hospital), the University of Melbourne, Parkville, Victoria, Australia. [14]Department of Biochemistry and Molecular Biology, Monash University, Clayton, Victoria, Australia.

Note: Supplementary data for this article are available at Cancer Discovery Online (http://cancerdiscovery.aacrjournals.org/).

Corresponding Author: Helen B. Pearson, European Cancer Stem Cell Research Institute, Haydn Ellis Building, Cardiff University, Cardiff CF24 4HQ, UK. Phone: 44-2920-688-517; E-mail: PearsonH2@cardiff.ac.uk

doi: 10.1158/2159-8290.CD-17-0867

INTRODUCTION

Prostate cancer is the second most common cause of male cancer-related death worldwide, emphasizing the failure of mainstay therapeutic regimens to treat advanced disease (1). A pivotal constraint for prostate cancer research is the lack of diverse *in vivo* models that accurately reflect the clinic. Expanding the range of prostate cancer models that display key clinicopathologic characteristics is vital to (i) delineate the complex molecular mechanisms underpinning prostate cancer, (ii) identify novel prognostic markers and therapeutic targets, and (iii) accurately establish the efficacy of novel therapies that are urgently needed in the clinic.

Class 1A PI3Ks are heterodimers consisting of a regulatory subunit encoded by *PIK3R1* (p85α/p55α/p50α), *PIK3R2* (p85β), or *PIK3R3* (p85γ), and a catalytic subunit encoded by *PIK3CA* (p110α), *PIK3CB* (p110β), or *PIK3CD* (p110δ; refs. 2, 3). Upon activation of receptor tyrosine kinases (RTK), G-protein–coupled receptors (GPCR), or RAS, PI3K is recruited to the membrane. Here, PI3K catalyzes the generation of the second messenger phosphatidylinositol(3,4,5)trisphosphate (PIP_3), which recruits the serine threonine kinases AKT [protein kinase B (PKB)] and PDK1 to the membrane, as well as a plethora of other PIP_3 binding proteins (4). The first identified, and most well studied, PIP_3 effector is AKT (4). PDK1 phosphorylates AKT at Thr308, leading to phosphorylation of downstream targets, including TSC2 that activates mTORC1 to promote proliferation, survival, and migration (2, 3). Phosphorylation of AKT at both Ser473 and Thr308 is required for the full activation of AKT and has been linked to coactivation of the mTORC1 and mTORC2 pathways (5). Key substrates of mTORC2 include AKT at Ser473 (5), and SGK1, which phosphorylates and inactivates the metastasis suppressor N-Myc–downregulated gene-1 (NDRG1/DRG1/CAP43; ref. 6). AKT dephosphorylation by PHLPP at Ser473 and PP2A at Thr308 deactivate AKT (5). The fine-tuning of AKT phosphorylation levels mediates AKT pathway activity and subsequent cellular events. In addition, the tumor suppressor PTEN serves to negatively regulate the PI3K cascade by catalyzing the dephosphorylation of PIP_3 to PIP_2. PTEN also mediates lipid phosphatase–independent tumor-suppressor activities via its protein phosphatase domain (2).

PI3K pathway hyperactivation is invariably associated with prostate cancer progression in the clinic, thus presenting an attractive therapeutic target. Indeed, loss of *PTEN*, a negative regulator of the PI3K pathway, is estimated to occur in 40% to 50% of patients with prostate cancer (7, 8). However, PI3K pathway hyperactivation can occur via a range of mechanisms (e.g., *PIK3CA* oncogenic mutation) that can independently influence downstream signaling events. We sought to determine if genetic drivers of the PI3K pathway that are present in prostate cancer, but have not been investigated previously, can also contribute to prostate cancer initiation/progression. To this end, we generated a new, clinically relevant genetically modified mouse model harboring a heterozygous activating mutation in *Pik3ca* specifically within prostate epithelial cells, and compared prostate histopathology with the

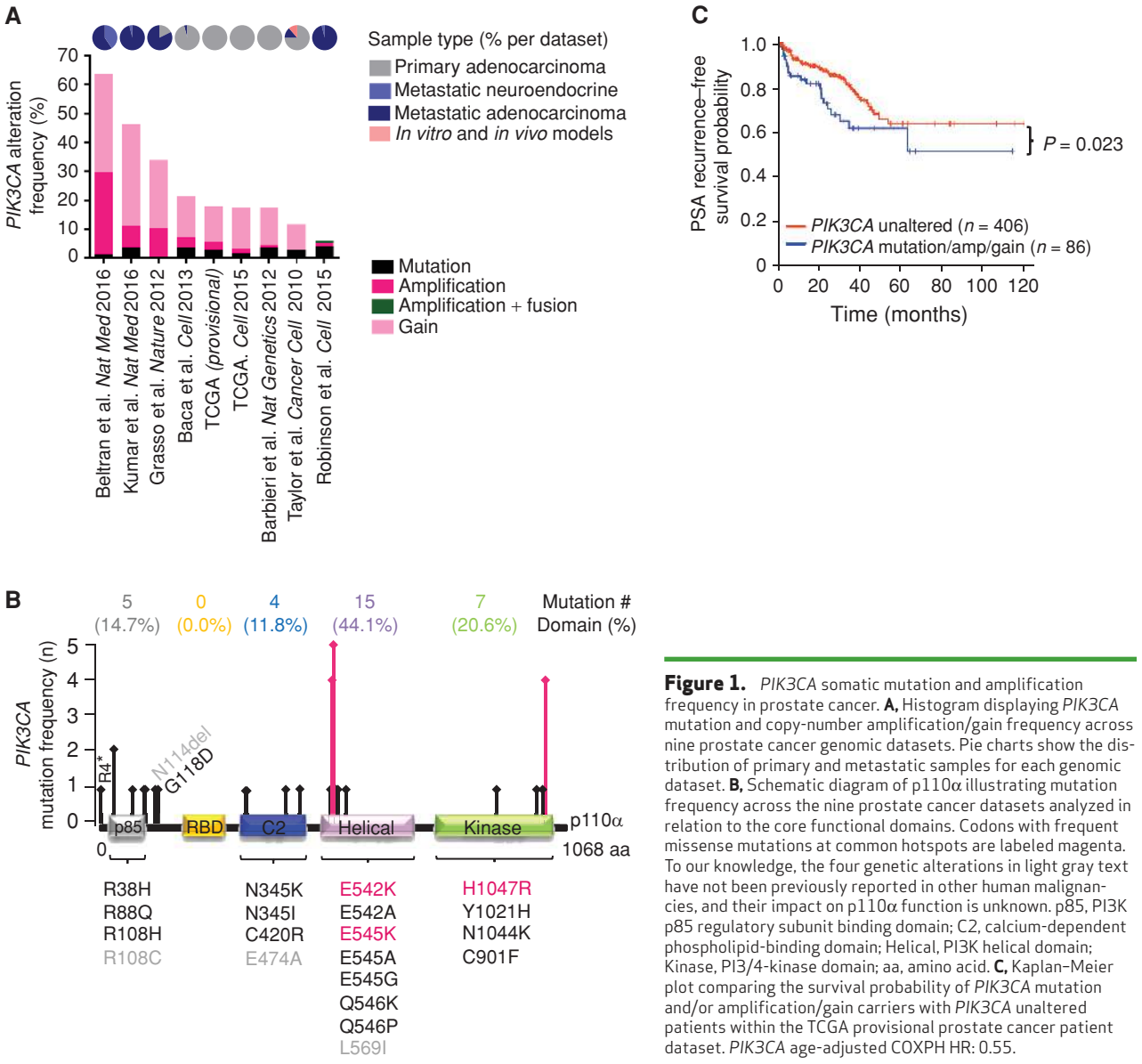

Figure 1. *PIK3CA* somatic mutation and amplification frequency in prostate cancer. **A,** Histogram displaying *PIK3CA* mutation and copy-number amplification/gain frequency across nine prostate cancer genomic datasets. Pie charts show the distribution of primary and metastatic samples for each genomic dataset. **B,** Schematic diagram of p110α illustrating mutation frequency across the nine prostate cancer datasets analyzed in relation to the core functional domains. Codons with frequent missense mutations at common hotspots are labeled magenta. To our knowledge, the four genetic alterations in light gray text have not been previously reported in other human malignancies, and their impact on p110α function is unknown. p85, PI3K p85 regulatory subunit binding domain; C2, calcium-dependent phospholipid-binding domain; Helical, PI3K helical domain; Kinase, PI3/4-kinase domain; aa, amino acid. **C,** Kaplan–Meier plot comparing the survival probability of *PIK3CA* mutation and/or amplification/gain carriers with *PIK3CA* unaltered patients within the TCGA provisional prostate cancer patient dataset. *PIK3CA* age-adjusted COXPH HR: 0.55.

well-characterized *Pten*-deleted mouse model of prostate cancer (9). Overall, our findings emphasize the prognostic value of PI3K genetic drivers to better inform personalized therapy design.

RESULTS

PIK3CA Mutation/Amplification Correlates with Advanced Prostate Cancer Progression

PIK3CA oncogenic mutation and amplification, which may increase p110α PI3K catalytic activity, are frequently detected in human cancers (10–13). To better understand the frequency of *PIK3CA* alterations in prostate cancer, we analyzed nine prostate cancer genomic datasets for *PIK3CA* mutations and gene amplification (14). Our analysis shows that *PIK3CA* mutations occur in up to 4% of patients with prostate cancer, whereas *PIK3CA* copy-number gain/amplification occurs in as many as 62% of cases (Fig. 1A; Supplementary Table S1). *PIK3CA* mutations were predominantly nucleotide missense substitutions (87.5%; Supplementary Fig. S1A) within the helical (44.1%) and kinase (20.6%) domains, and previously reported hotspot mutations in exons 9 (E542K, E545K) and 20 (H1047R; refs. 10–12, 15) were most frequent (Fig. 1B). Notably, the majority of *PIK3CA* mutations observed (83%, 19/23) have been previously detected in prostate or nonprostate malignancies (12, 13, 15, 16), and are reported to increase p110α activity (refs. 12, 15–18; Fig. 1B).

To determine if *PIK3CA* mutation/amplification correlates with prostate cancer progression, we analyzed The Cancer Genome Atlas (TCGA) provisional prostate cancer dataset (Supplementary Table S2). Our analysis revealed that *PIK3CA* mutation and copy-number gain/amplification frequency significantly correlates with poor prostate cancer survival, regional lymph node metastasis, and a higher primary tumor category and Gleason grade (Fig. 1C; Supplementary Table S3), resembling *PTEN* loss (Supplementary Fig. S1B; Supplementary Table S4).

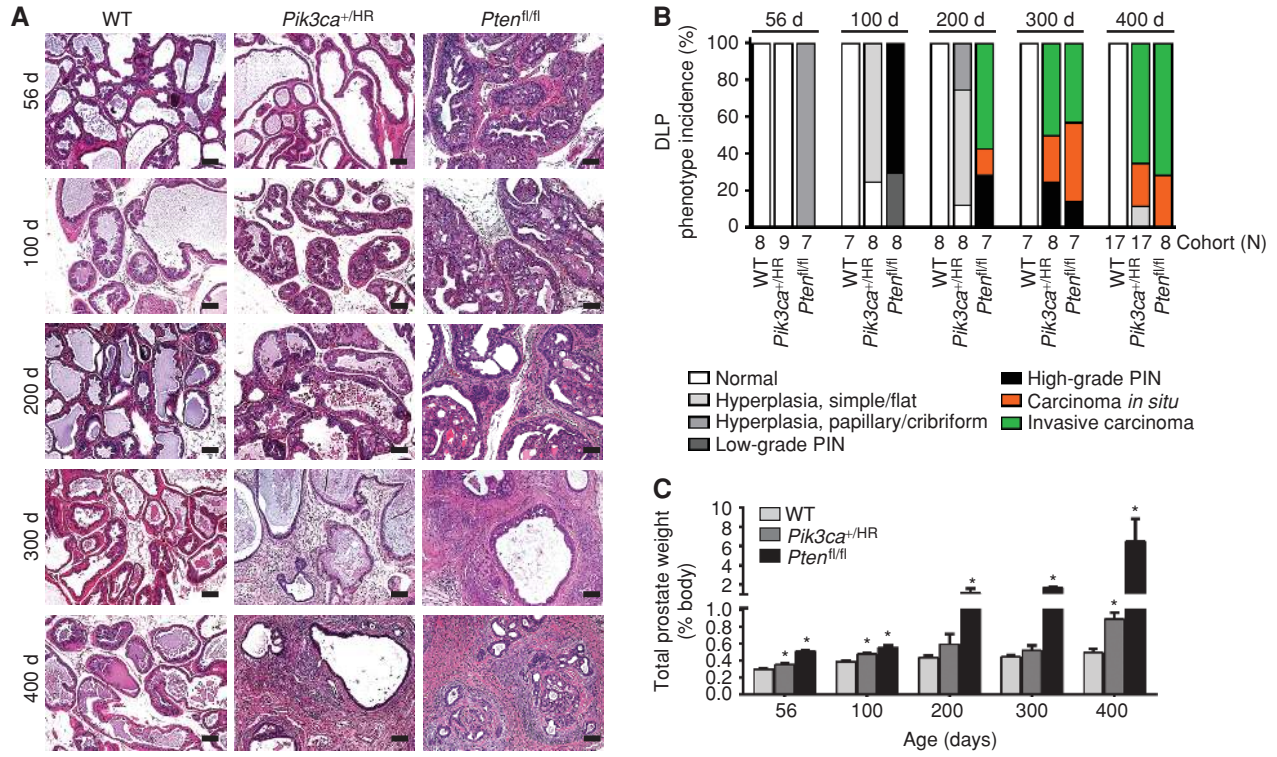

Figure 2. Heterozygous *Pik3ca*^{H1047R} oncogenic mutation causes invasive prostate cancer in mice that does not phenocopy *Pten* deletion. **A,** Representative hematoxylin/eosin images of WT, *Pik3ca*$^{+/HR}$, and *Pten*$^{fl/fl}$ dorsolateral prostate epithelium (scale bar, 100 μm). **B,** Histogram displaying phenotype incidence in WT, *Pik3ca*$^{+/HR}$, and *Pten*$^{fl/fl}$ dorsolateral prostate. DLP, dorsolateral prostate. **C,** Bar graph displaying total prostate weight normalized to body weight for WT, *Pik3ca*$^{+/HR}$, and *Pten*$^{fl/fl}$ mice. *n* = as indicated (*N*). Error bars, SEM, *, $P < 0.05$ compared with WT, one-way ANOVA with Tukey multiple comparison test.

Coexpression analysis within the 9 prostate cancer datasets analyzed revealed that 39.4% (13/33 patients) of *PIK3CA* mutation carriers also harbored *PTEN* mutation or copy-number loss, indicating that patients with *PIK3CA*-mutant prostate cancer have a high frequency of coexistent *PTEN* deleterious genetic alterations, consistent with ovarian, breast, endometrial, and colorectal cancer studies (11, 19, 20). Interestingly, 47.5% (96/202) of patients with prostate cancer with *PIK3CA* amplification/gain also carried a *PTEN* mutation or copy-number loss. Moreover, statistical analysis of the larger TCGA provisional dataset revealed a significant tendency toward *PIK3CA* mutation/amplification/gain and *PTEN* mutation/loss co-occurrence in patients with prostate cancer ($P < 0.001$, Fisher exact test, Log OR = 0.916). Together, these findings suggest that *PIK3CA* mutation/amplification/gain play an oncogenic role during prostate cancer and indicate that p110α gain of function and *PTEN* loss may cooperate to promote prostate cancer growth.

Pik3ca^{H1047R} Mutation in Mouse Prostate Epithelium Causes Locally Invasive Prostate Carcinoma

To delineate the oncogenic role of a clinically relevant *PIK3CA* mutation within the prostate, we intercrossed mice that harbor a conditional latent H1047R mutation in *Pik3ca* to the *PBiCre* transgenic line. Using an exon-switch Cre-LoxP approach, expression of *Pik3ca*^{H1047R} was driven specifically within the prostate following *PBiCre*-mediated excision of the floxed wild-type (WT) *Pik3ca* exon 20 and subsequent expression of a latent downstream mutant exon 20 (11, 21). Recombination was confirmed by sequencing and allele-specific PCR analysis of cDNA isolated from the prostate glands of *PBiCre*$^{+/-}$;*Pik3ca*$^{+/+}$ and *PBiCre*$^{+/-}$;*Pik3ca*$^{+/Lat\text{-}H1047R}$ mice, hereafter referred to as WT and *Pik3ca*$^{+/HR}$, respectively (Supplementary Fig. S2A and S2B). Histologic analysis of WT and *Pik3ca*$^{+/HR}$ prostate lobes revealed no gross phenotype in WT mice, whereas *Pik3ca*$^{+/HR}$ cohorts displayed a progressive malignant phenotype. *Pik3ca*$^{+/HR}$ mice developed multifocal simple and/or cribriform hyperplasia in all prostate lobes by 100 days and homogeneous, locally invasive prostate carcinoma by 300 to 400 days (dorsolateral lobe, Fig. 2A and B; ventral/anterior lobes, Supplementary Fig. S2C–S2E and Supplementary Table S5). Invasion was confirmed by the absence of smooth muscle actin (SMA) staining by immunohistochemistry (IHC; Supplementary Fig. S2F). *Pik3ca*$^{+/HR}$ prostate carcinomas were predominantly dysplastic/mucinous, and reactive stroma and immune infiltrate were evident (Fig. 2A; 300–400 days; Supplementary Fig. S2C). Taken together, these data demonstrate that heterozygous *Pik3ca*^{H1047R} oncogenic mutation is sufficient to cause invasive prostate cancer in mice and to our knowledge is the first example of a monoallelic mutation driving invasive prostate cancer growth *in vivo*.

To determine if the genetic driver of the PI3K cascade influences prostate tumorigenesis and/or malignant progression, we compared our novel *Pik3ca*$^{+/HR}$ prostate cancer model with the well-characterized *Pten*-deleted mouse model of prostate

cancer (9). To this end, we generated age-matched cohorts of *PBiCre*$^{+/-}$;*Pten*$^{fl/fl}$ mice (denoted *Pten*$^{fl/fl}$) deficient for both copies of *Pten* within prostate epithelial cells and compared the phenotype on the same genetic background. In contrast to *Pik3ca*$^{+/HR}$ mice, we observed early onset of hyperplastic lesions at 56 days and rapid tumor progression from prostate intraepithelial neoplasia (PIN) to locally invasive carcinoma in *Pten*$^{fl/fl}$ mice by 200 days (Fig. 2A and B; Supplementary Fig. S2C–S2E; Supplementary Table S5). Furthermore, *Pten*$^{fl/fl}$ prostate tumor burden was significantly greater and more heterogeneous than the *Pik3ca*$^{+/HR}$ model (Fig. 2A and C), as carcinosarcomas were also present by 300 days in 29% of the cohort (2/7). However, metastasis to the liver, lung, lymph nodes, or bone was not detected in either model. *Pten*$^{fl/fl}$ mice were also prone to seminal vesicle neoplasia, urethra neoplasia, and adrenal pheochromocytoma that were rare, or absent, in *Pik3ca*$^{+/HR}$ mice (Supplementary Table S5). These findings indicate that relative to the *Pik3ca*$^{+/HR}$ model, early disease onset and potentially accelerated progression contribute to the earlier emergence of invasive carcinoma in *Pten*$^{fl/fl}$ mice.

To investigate if *Pten* biallelic loss accelerates prostate tumor growth compared with *Pik3ca*$^{+/HR}$-driven prostate cancer, we performed and quantitated IHC to detect the S-phase proliferation marker PCNA. *Pik3ca*$^{+/HR}$ prostate disease (100–400 days) showed a significant increase in the number of PCNA-positive proliferating cells compared with WT controls; however, a clear proliferation advantage was evident in *Pten*$^{fl/fl}$ mice between 56 and 200 days (Fig. 3A and B). Furthermore, significantly more PCNA-positive cells were detected in *Pten*$^{fl/fl}$ prostate hyperplasia compared with *Pik3ca*$^{+/HR}$ hyperplastic lesions (Supplementary Fig. S2G), indicating this is an early phenomenon during disease progression. These data show that increased proliferation in *Pten*$^{fl/fl}$ mice facilitates accelerated prostate cancer progression compared with *Pik3ca*$^{+/HR}$ mice. Notably, apoptosis evasion is not likely to contribute to accelerated disease progression in *Pten*$^{fl/fl}$ mice, as the number of cleaved caspase-3 (CC3)–positive apoptotic cells was largely increased in *Pten*$^{fl/fl}$ prostate epithelium compared with age-matched *Pik3ca*$^{+/HR}$ mutants (Supplementary Fig. S3A and S3B). IHC analysis to detect prostate basal and luminal cell markers, cytokeratin-5 (CK5) and cytokeratin-8 (CK8), respectively, revealed that, unlike *Pten*$^{fl/fl}$ prostate tumors, *Pik3ca*$^{+/HR}$-driven tumors are predominantly comprised of luminal epithelial cells and rarely display expansion/mislocalization of the CK5-positive basal cell population (Supplementary Fig. S3C). Taken together, these data show that although a single *Pik3ca*^{H1047R} activating mutation predisposes to murine prostate cancer, like biallelic loss of *Pten*, these two genetic drivers of the PI3K cascade do not completely phenocopy. Overall, these findings suggest that *Pik3ca* oncogenic mutation and *Pten* loss may drive prostate tumor phenotypes via distinct molecular mechanisms, which could present novel therapeutic targets.

Pik3ca Mutation and *Pten* Loss Stimulate mTORC1 Signaling to Promote Prostate Tumorigenesis and Facilitate Malignant Progression in Mice

Given that both *Pten* deletion and *Pik3ca* oncogenic mutations can activate PI3K signaling, the phenotypic differences observed between the genetic drivers could reflect differential activation of the PI3K cascade. To determine if PTEN tumor-suppressive function is maintained in the *Pik3ca*$^{+/HR}$ model, we performed IHC to detect PTEN. We observed uniform membranous PTEN staining in WT prostate epithelium and *Pik3ca*$^{+/HR}$ tumors, whereas PTEN-positive cells were absent in *Pten*$^{fl/fl}$ prostate tumors, consistent with biallelic *Pten* ablation (Fig. 3C). To determine if PTEN impairs effector cascades downstream of PI3K in the *Pik3ca*$^{+/HR}$ model to delay prostate tumorigenesis and progression, we evaluated AKT activation and the status of the PI3K downstream mTOR effector cascades. mTOR is a serine/threonine kinase that forms part of two distinct complexes, mTORC1 and mTORC2. We show that the number of prostate epithelial cells displaying activation of AKT via Thr308 phosphorylation at the cell membrane is significantly increased in *Pik3ca*$^{+/HR}$ and *Pten*$^{fl/fl}$ prostate carcinoma compared with WT controls (Fig. 3C and D), indicating that both PI3K genetic drivers stimulate mTORC1 signaling to promote tumor growth. In support, the proportion of cells displaying phosphorylation of well-known downstream mTORC1 targets, namely the ribosomal protein S6 (RPS6) at Ser235/236 that regulates cell size and proliferation and 4e-binding protein 1 (4E-BP1) at Thr37/46 that mediates translational machinery, were also significantly elevated in both models (Fig. 3C, E–F). Our analysis of the number of pAKT Thr308-, pRPS6-, and p4E-BP1–positive cells in *Pten*$^{fl/fl}$ and *Pik3ca*$^{+/HR}$ hyperplastic lesions also revealed that mTORC1 signaling upregulation occurs premalignancy (Supplementary Fig. S3D–S3G). Of note, the number of pRPS6- and p4E-BP1–positive cells was comparable in *Pik3ca*-mutated and *Pten*-deleted hyperplastic lesions and advanced tumors, despite significantly more pAKT Thr308-positive cells being detected in the *Pten*$^{fl/fl}$ model, suggesting that pAKT Thr308–independent phosphorylation of RPS6 and 4E-BP1 may occur, or that the partial increase in pAKT Thr308 in *Pik3ca*$^{+/HR}$ tumors is sufficient to sustain pRPS6 and p4E-BP1 signaling. Taken together, these data indicate that both *Pik3ca*^{H1047R} oncogenic mutation and *Pten* biallelic loss stimulate mTORC1 signaling to facilitate prostate tumor formation and progression, and that PTEN-mediated tumor-suppressive functions do not impair mTORC1 downstream signaling in the context of *Pik3ca* mutation.

Relative to *Pik3ca* Mutation, *Pten* Deletion Augments mTORC2 Signaling to Further Promote Prostate Tumor Formation and Progression in Mice

Because activation of the mTORC1 downstream targets was comparable between *Pik3ca*$^{+/HR}$ and *Pten*$^{fl/fl}$ prostate cancer models, we reasoned that the early onset and accelerated progression observed in the *Pten*$^{fl/fl}$ model may be attributable to mTORC2 signaling. To investigate this, we performed and quantitated IHC in *Pik3ca*$^{+/HR}$ and *Pten*$^{fl/fl}$ prostate carcinomas to detect the phosphorylation of two mTORC2 targets: AKT at Ser473 and NDRG1 at Thr346. We show that the number of pAKT Ser473– and pNDRG1 Thr346–positive cells was significantly increased in *Pten*$^{fl/fl}$ prostate tumors compared with the *Pik3ca*$^{+/HR}$ model and WT controls (Fig. 3C, G–H). Similar results were observed when comparing hyperplastic lesions (Supplementary Fig. S3D, S3H, and S3I). Thus, mTORC2

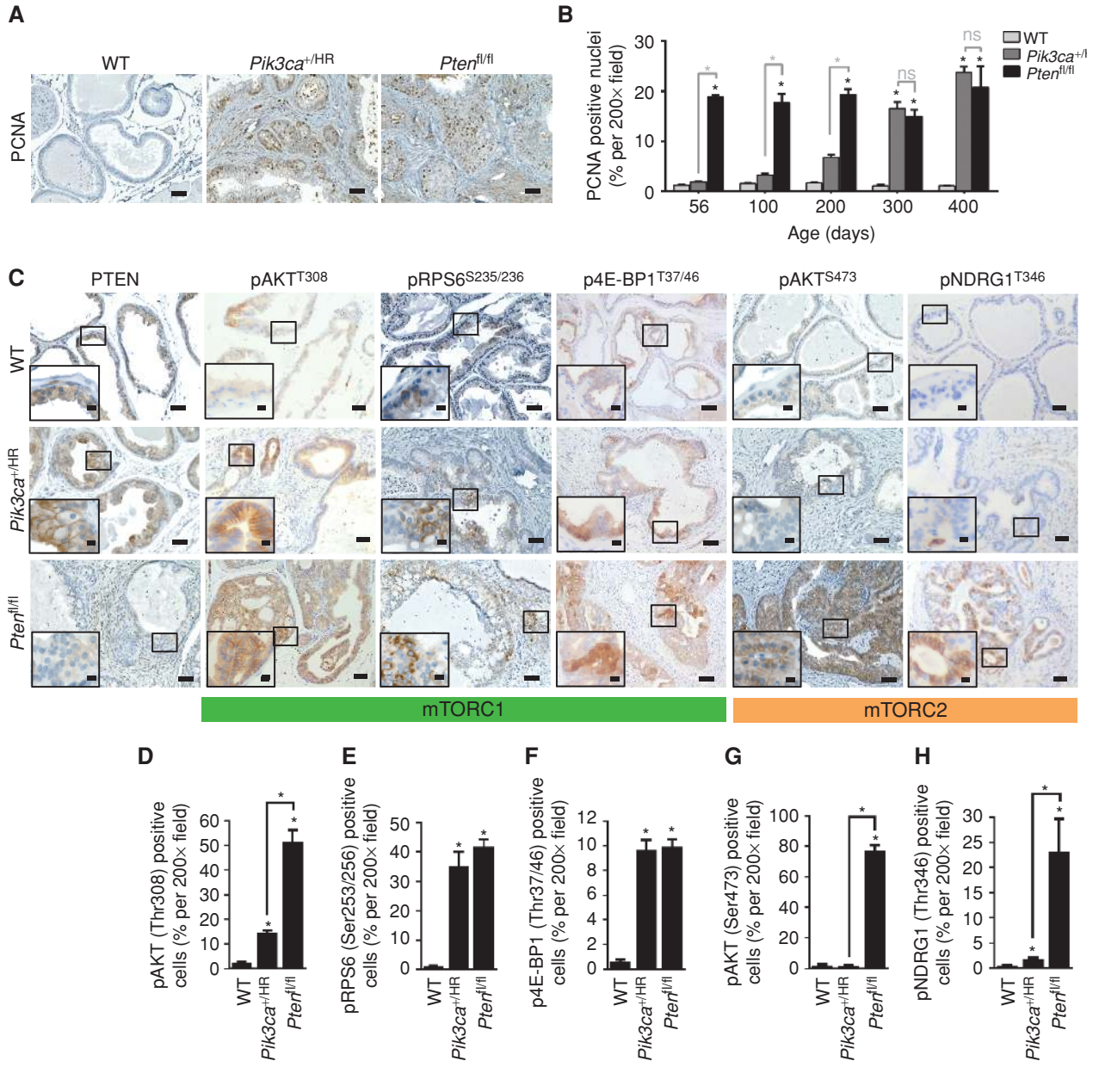

Figure 3. *Pten* deletion triggers mTORC2 signaling to facilitate rapid prostate cancer progression relative to *Pik3ca*^{H1047R} mutation. **A,** IHC to detect the proliferation marker PCNA in WT, *Pik3ca*$^{+/HR}$, and *Pten*$^{fl/fl}$ prostate carcinoma at 400 days of age. Scale bars, 50 μm. **B,** Quantitation of PCNA-positive nuclei in WT, *Pik3ca*$^{+/HR}$, and *Pten*$^{fl/fl}$ prostate epithelium ($n = 3$, *, $P < 0.05$ compared with WT, or as indicated, one-way ANOVA with Tukey multiple comparison test; error bars, SEM). **C,** Representative IHC images to detect PTEN, mTORC1 signaling components (pAKT Thr308, pRPS6 Ser235/236, and p4E-BP1 Thr37/46), and mTORC2 substrates (pAKT Ser473 and pNDRG1 Thr346) in WT dorsolateral prostate and *Pik3ca*$^{+/HR}$ and *Pten*$^{fl/fl}$ prostate carcinoma at 400 days of age ($n = 3$; scale bar, 50 μm; inset scale bar, 10 μm). IHC quantitation for (**D**) pAKT Thr308, (**E**) pRPS6 Ser235/236, (**F**) p4E-BP1 Thr37/46, (**G**) pAKT Ser473, and (**H**) pNDRG1 Thr346 in WT dorsolateral prostate and *Pik3ca*$^{+/HR}$ and *Pten*$^{fl/fl}$ prostate carcinoma at 400 days of age ($n = 3$; error bars, SEM; *, $P < 0.05$ compared with WT, or as indicated, one-way ANOVA with Tukey multiple comparison correction).

signaling presents a direct mechanism whereby *Pten* homozygous deletion can promote tumor onset/progression relative to *Pik3ca*^{H1047R} oncogenic mutation in this setting.

Pik3ca^{H1047R} Mutation Causes p110α-Dependent Prostate Cancer

Recent reports have demonstrated that p110α and p110β isoforms of the PI3K catalytic subunit play distinct cellular functions and are regulated independently by differential binding partners (22–25). For instance, *in vitro* assays have established that RAS subfamily members can directly bind to the RAS binding domain (RBD) of p110α (and not p110β) to activate p110α kinase activity, and p110β RBD:RAC1 interactions have been shown to be required for GPCR-mediated p110β signaling (22–24). Moreover, *Pten*-deleted prostate cancers are considered to preferentially activate the p110β

isoform, and p110β blockade has been shown to activate p110α owing to relief of feedback inhibition (e.g., via IGF1R; refs. 25–28). Thus, we sought to determine if the phenotypic difference between *Pten* loss and *Pik3ca* oncogenic mutation reflects differential activation of PI3K catalytic isoforms. To this end, we performed IHC to detect pERK, a downstream target of the RAS cascade, and activation of RAC1 GTPase in *Pik3ca*$^{+/HR}$ and *Pten*$^{fl/fl}$ prostate tumors to distinguish activation of RAS–p110α and RAC1–p110β signaling axes, respectively. We find that pERK expression is markedly elevated in *Pik3ca*$^{+/HR}$ and *Pten*$^{fl/fl}$ prostate tumors compared with age-matched WT controls, indicating p110α signaling is activated in both models (Fig. 4A). However, only *Pten*$^{fl/fl}$ prostate tumors displayed Active RAC1–GTP staining (Fig. 4B), indicating that activation of p110β signaling may promote prostate cancer growth induced by *Pten* deletion.

To directly test p110α and p110β isoform dependency in *Pik3ca*-mutant and *Pten*-deleted prostate cancers, we administered isoform-specific inhibitors (A66, a p110α-specific inhibitor, or TGX-221, a p110β-specific inhibitor) or a pan-PI3K inhibitor (BKM120) to cohorts of *Pik3ca*$^{+/HR}$ and *Pten*$^{fl/fl}$ mice with prostate carcinoma for 4 weeks. *Pik3ca*$^{+/HR}$ tumor burden regressed significantly in response to A66 and BKM120, whereas TGX-221 had no effect, indicative of p110α dependency (Fig. 4C). In contrast, *Pten*$^{fl/fl}$ tumor burden was not reduced upon single isoform-specific inhibitor treatment but did respond to BKM120 or combined A66 and TGX-221 therapy, suggesting *Pten*-deleted tumors are p110β/p110α codependent (Fig. 4D). Histopathologic analysis of prostate lobes confirmed tumor regression in A66- and BKM120-treated *Pik3ca*$^{+/HR}$ mice and BKM120- and A66+TGX-221-treated *Pten*$^{fl/fl}$ mice (Fig. 4E; Supplementary Fig. S4A–S4C). These data suggest that p110β-mediated signaling events could facilitate *Pten*-deleted prostate cancer but not *Pik3ca*^{H1047R}-mutated prostate cancer, and support previous work showing that combined p110α and p110β blockade improves therapeutic outcome in *PTEN*-deficient prostate cancers compared with PI3K isoform–specific monotherapy (22, 26, 28). Indeed, PI3K pathway inhibitors on their own have been shown to have limited efficacy in the clinic due to multiple feedback loops, PI3K-independent pathways, and/or additional oncogenic mutations, and can cause side effects (e.g., hyperglycemia; refs. 22, 26, 28, 29). Thus, treatment approaches that combine PI3K pathway inhibitors with other therapeutic agents are currently being explored to improve outcomes for patients with prostate cancer.

Pten Deletion and *Pik3ca*$^{+/HR}$ Mutation Cooperate to Accelerate Prostate Cancer Progression in Mice

Given that we have found that *PIK3CA* mutation and *PTEN* loss are not mutually exclusive events in patients with prostate cancer, we sought to generate a new clinically relevant model of prostate cancer and to test if PI3K genetic drivers can cooperate to facilitate prostate cancer growth. Hence, we crossed *Pik3ca*$^{+/HR}$ mutants with *Pten*$^{fl/fl}$ animals to develop *PBiCre*$^{+/-}$;*Pik3ca*$^{+/HR}$;*Pten*$^{fl/fl}$ compound mutants (termed *Pik3ca*$^{+/HR}$;*Pten*$^{fl/fl}$) that harbor *Pik3ca*$^{+/HR}$ mutation and biallelic *Pten* loss in prostate epithelial cells. At 56 and 100 days, we observed aggressive, locally invasive carcinoma with 100% incidence in all *Pik3ca*$^{+/HR}$;*Pten*$^{fl/fl}$ prostate lobes (Fig. 5A and B; Supplementary Fig. S5A and S5B; Supplementary Table S5). IHC analysis revealed that *Pik3ca*$^{+/HR}$;*Pten*$^{fl/fl}$ prostate tumors resemble *Pten*$^{fl/fl}$ tumors, where the CK5^{+} basal cell population is expanded/mislocalized and the CK8^{+} luminal cells are predominant (Supplementary Fig. S5C). Local invasion was confirmed by the absence of SMA staining (Supplementary Fig. S5C). Tumor burden was also significantly greater in compound mutants than age-matched single mutants (Supplementary Fig. S5D). Visceral metastases were not detected by 100 days of age, and the development of nonprostate malignancies reflecting leaky *PBiCre*-mediated recombination (predominantly benign buccal mucosal/cutaneous papillomas and penile prolapse) prevented further aging of *Pik3ca*$^{+/HR}$;*Pten*$^{fl/fl}$ mice.

To investigate the mechanism underpinning cooperation between *Pik3ca* mutation and *Pten* loss, we determined the number of proliferative and apoptotic cells in *Pik3ca*$^{+/HR}$, *Pten*$^{fl/fl}$, and *Pik3ca*$^{+/HR}$;*Pten*$^{fl/fl}$ locally invasive prostate carcinomas by PCNA and CC3 IHC, respectively. We show that compound-mutant tumors have significantly more PCNA-positive proliferating cells than single mutants (Fig. 5C and D), whereas CC3-mediated apoptosis is unaltered (Supplementary Fig. S5E and S5F). These findings indicate that *Pik3ca* oncogenic mutation and *Pten* loss synergize to accelerate prostate cancer progression by increasing proliferation, but not survival.

To ascertain if the increased proliferation in *Pik3ca*$^{+/HR}$;*Pten*$^{fl/fl}$ mice reflects further activation of mTORC1/2 signaling, we performed IHC to detect pAKT Thr308 that leads to mTORC1 activation, as well as the phosphorylation of known mTORC1/2 downstream signaling targets. Quantitation of IHC staining revealed that the number of cells expressing membranous pAKT Thr308 is significantly increased in *Pik3ca*$^{+/HR}$;*Pten*$^{fl/fl}$ prostate carcinomas compared with stage-matched single mutants (Fig. 5E; Supplementary Fig. S5G). In accordance, the mTORC1 downstream targets pRPS6 and p4E-BP1 positively correlated with pAKT Thr308 activation (Fig. 5F and G; Supplementary Fig. S5G), indicating increased mTORC1 signaling accelerates prostate cancer growth in *Pik3ca*$^{+/HR}$;*Pten*$^{fl/fl}$ mutants. Phosphorylation of the mTORC2 downstream targets pAKT Ser473 and pNDRG1 was also significantly increased in compound mutants compared with single mutants (Fig. 5H and I; Supplementary Fig. S5G). Taken together, these findings suggest that further potentiation of mTORC1 and mTORC2 signaling, which correlates with superactivation of AKT at Thr308/Ser473, contributes to the cooperative relationship between *Pik3ca* mutation and *Pten* loss during prostate cancer in this setting.

Previous work has shown that amplification/overexpression of *Pik3ca* and *Pik3cb* increases oncogenicity (22, 30, 31), and amplification frequently correlates with poor patient outcome in multiple malignancies (22). To establish if *Pik3ca/b* transcripts are expressed at physiologic levels in *Pik3ca*$^{+/HR}$, *Pten*$^{fl/fl}$, and *Pik3ca*$^{+/HR}$;*Pten*$^{fl/fl}$ prostate carcinomas, we performed RNA *in situ* hybridization and quantitated RNA molecules relative to WT controls. We show that *Pik3ca* and *Pik3cb* mRNA is significantly increased in double-mutant prostate tumors compared with *Pten*$^{fl/fl}$ and *Pik3ca*$^{+/HR}$ single-mutant tumors and age-matched WT controls (Fig. 5J–L; Supplementary Fig. S5H). However, the functional consequences of *Pik3ca* and *Pik3cb* mRNA upregulation remain elusive.

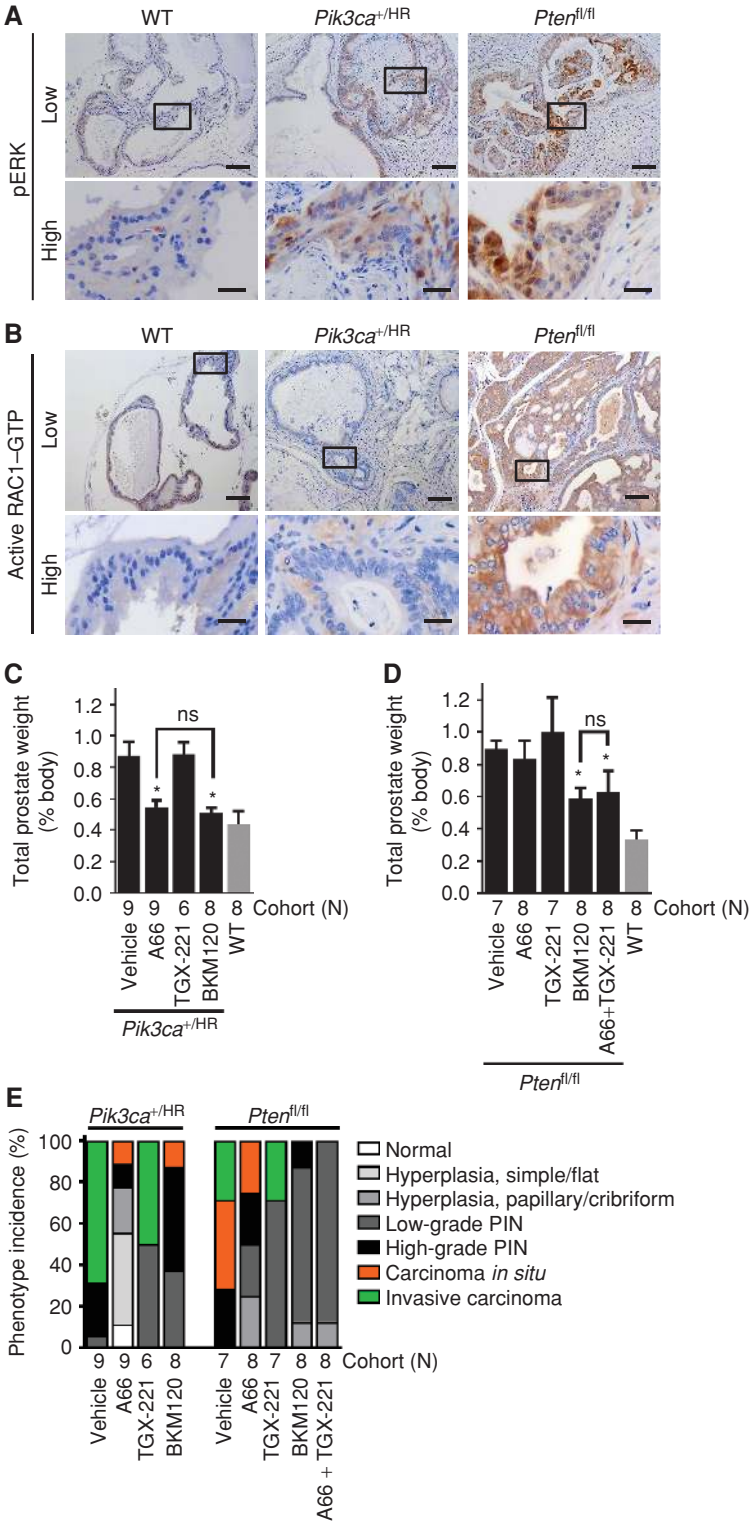

Figure 4. *Pik3ca*$^{+/HR}$ prostate cancer is p110α-dependent, whereas *Pten*$^{fl/fl}$ prostate cancer is p110α and p110β codependent. Representative IHC images to detect (**A**) pERK Thr202/Tyr204 and (**B**) Active RAC1-GTP in WT dorsolateral prostate and *Pik3ca*$^{+/HR}$ and *Pten*$^{fl/fl}$ prostate carcinoma at 400 days of age ($n = 3$; low-magnification scale bar, 100 μm; high-magnification scale bar, 10 μm). Bar graph indicating total prostate weight normalized to body weight for *Pik3ca*$^{+/HR}$ mice (**C**) and *Pten*$^{fl/fl}$ mice (**D**) with prostate carcinoma administered with either vehicle, p110α-specific inhibitor (A66), p110β-specific inhibitor (TGX-221), pan-PI3K inhibitor (BKM120), or A66 + TGX-221 for 4 weeks compared with age-matched WT controls. n = as indicated (N). Error bars, SEM; *, $P < 0.05$ compared with vehicle, one-way ANOVA with Tukey multiple comparison correction; ns, not significant. **E,** Histogram displaying phenotype incidence for dorsolateral prostate from *Pik3ca*$^{+/HR}$ and *Pten*$^{fl/fl}$ mice treated with either vehicle, p110α-specific inhibitor (A66), p110β-specific inhibitor (TGX-221), pan-PI3K inhibitor (BKM120), or A66 + TGX-221 for 4 weeks.

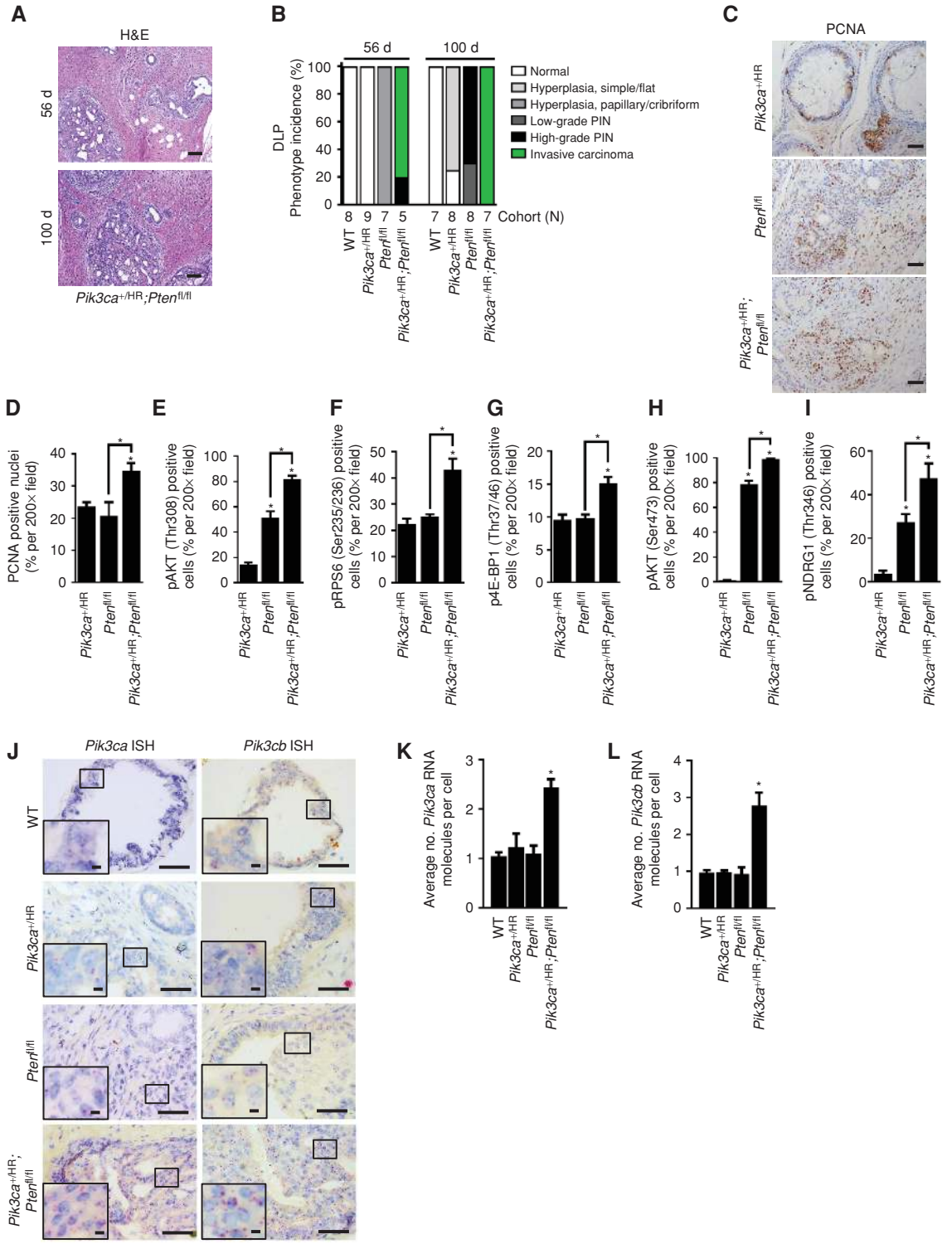

Figure 5. *Pik3ca* mutation and *Pten* loss cooperate to accelerate prostate cancer progression in mice by upregulating proliferation and mTORC1/2 signaling. **A,** Representative IHC images of *Pik3ca*$^{+/HR}$;*Pten*$^{fl/fl}$ prostate carcinoma at 56 and 100 days of age. Scale bars, 100 μm. **B,** Phenotype incidence histogram for WT, *Pik3ca*$^{+/HR}$, *Pten*$^{fl/fl}$, and *Pik3ca*$^{+/HR}$;*Pten*$^{fl/fl}$ dorsolateral prostate at 56 and 100 days of age. **C,** IHC to detect PCNA in *Pik3ca*$^{+/HR}$, *Pten*$^{fl/fl}$, and *Pik3ca*$^{+/HR}$;*Pten*$^{fl/fl}$ stage-matched prostate carcinomas. Scale bars, 50 μm. IHC quantitation for (**D**) PCNA, (**E**) pAKT Thr308, (**F**) pRPS6 Ser235/236, (**G**) p4E-BP1 Thr37/46, (**H**) pAKT Ser473, and (**I**) pNDRG1 Thr346 in *Pik3ca*$^{+/HR}$, *Pten*$^{fl/fl}$, and *Pik3ca*$^{+/HR}$;*Pten*$^{fl/fl}$ stage-matched prostate carcinomas ($n = 3$; *, $P < 0.05$ compared with *Pik3ca*$^{+/HR}$ or as indicated, one-way ANOVA with Tukey correction; error bars, SEM). **J,** RNA *in situ* hybridization (ISH) analysis of *Pik3ca* and *Pik3cb* transcripts in *Pik3ca*$^{+/HR}$, *Pten*$^{fl/fl}$, and *Pik3ca*$^{+/HR}$;*Pten*$^{fl/fl}$ stage-matched prostate carcinomas ($n = 3$; scale bars, 50 μm; inset scale bars, 5 μm). Quantitation of (**K**) *Pik3ca* and (**L**) *Pik3cb* mRNA molecules detected by *in situ* hybridization in *Pik3ca*$^{+/HR}$, *Pten*$^{fl/fl}$, and *Pik3ca*$^{+/HR}$; *Pten*$^{fl/fl}$ stage-matched prostate carcinomas ($n = 3$; *, $P < 0.05$ compared with WT, one-way ANOVA with Tukey correction; error bars, SEM).

Pik3ca$^{+/HR}$- and *Pten*$^{fl/fl}$-Induced Prostate Cancers Acquire CRPC in Mice

PTEN loss is widely reported to correlate with resistance to androgen deprivation therapy in patients with prostate cancer and mice (9, 32, 33). To examine if *Pik3ca*$^{+/HR}$-driven prostate cancer also confers castration-resistant disease, we aged cohorts of *Pik3ca*$^{+/HR}$-mutant mice until invasive prostate carcinoma had developed (300 days) and assessed the early and long-term response to surgical castration. Although we observed a significant reduction in *Pik3ca*$^{+/HR}$ total prostate weight at 2 and 10 weeks after castration (Fig. 6A), histopathologic analysis revealed that prostate tumors were still present in *Pik3ca*$^{+/HR}$ mice, indicating the development of acquired castration-resistant prostate cancer (CRPC; Fig. 6B; Supplementary Fig. S6A). These findings are in keeping with partial androgen sensitivity and the latent acquisition of CRPC, mirroring homozygous deletion of *Pten* (Fig. 6A and B; Supplementary Fig. S6A), as previously reported (33, 34). IHC to detect androgen receptor (AR) confirmed the reduction of androgens after castration, as cytoplasmic AR was detected in *Pik3ca*$^{+/HR}$ and *Pten*$^{fl/fl}$ prostate epithelial cells following castration, whereas uncastrated controls displayed active nuclear AR (Supplementary Fig. S6B).

To determine if *Pik3ca* heterozygous oncogenic mutation sensitizes preneoplastic prostate epithelium to CRPC transition, we examined the short-term and long-term response of *Pik3ca*$^{+/HR}$ mice to castration at 100 days, when only hyperplastic disease is present. Prostate epithelial regression was detected 2 weeks after castration and correlated with a reduction in prostate weight, yet small prostate hyperplastic and dysplastic tumors, resembling uncastrated *Pik3ca*$^{+/HR}$ mutants, had developed by 42 weeks after castration in 100% (6/6) and 67% (4/6) of cases, respectively (Supplementary Fig. S6C and S6D). These data demonstrate that *Pik3ca*-mutated prostate epithelium possesses an inherent ability to acquire CRPC, similarly to *Pten* loss (9).

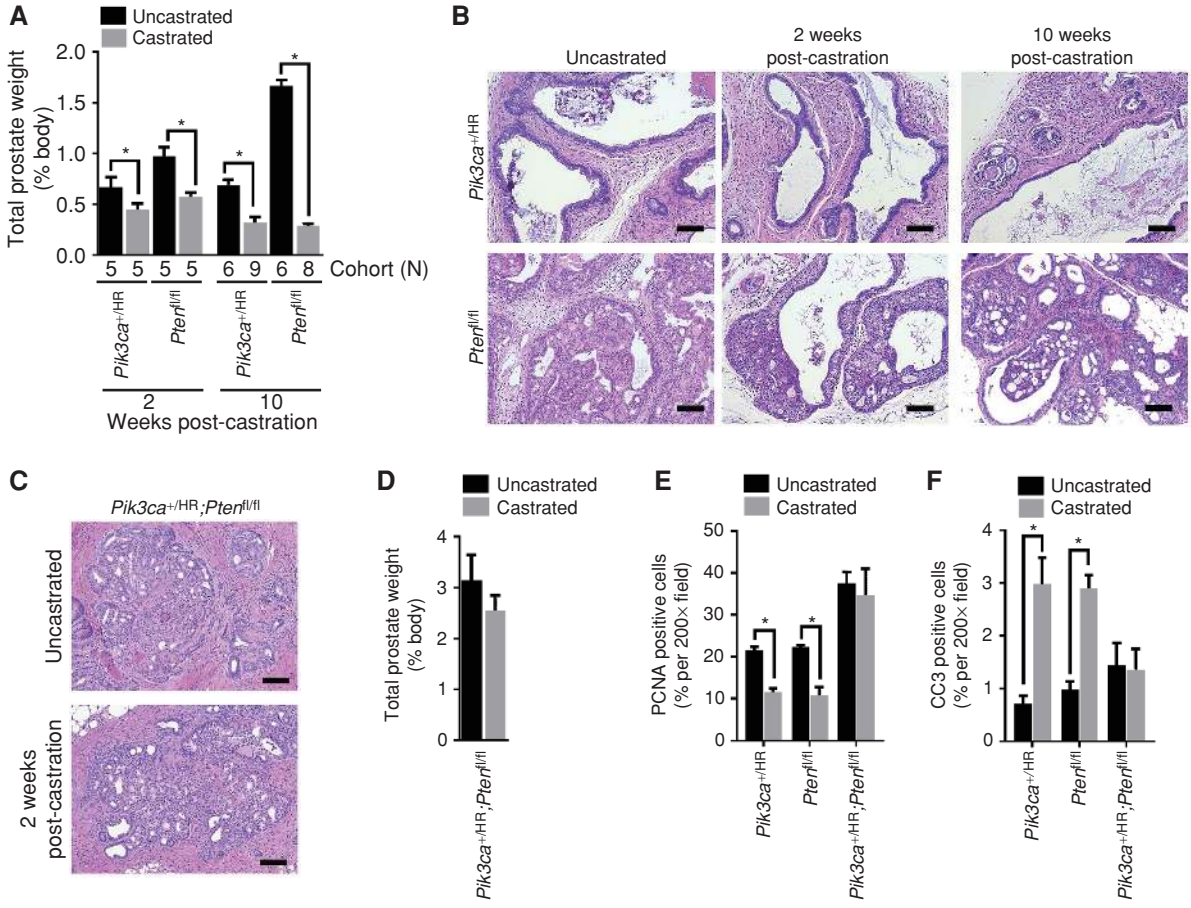

Figure 6. *Pik3ca*$^{+/HR}$ and *Pten*$^{fl/fl}$ prostate cancers acquire CRPC, whereas *Pik3ca*$^{+/HR}$;*Pten*$^{fl/fl}$ compound mutants display innate resistance to castration. **A,** Bar graph displaying total prostate weight normalized to body weight for *Pik3ca*$^{+/HR}$ and *Pten*$^{fl/fl}$ mice 2 and 10 weeks after castration relative to age-matched/uncastrated controls. *n* = as indicated (*N*); error bars, SEM; *, $P < 0.05$, one-way ANOVA with Tukey correction. **B,** Representative hematoxylin/eosin (H&E) images of *Pik3ca*$^{+/HR}$- and *Pten*$^{fl/fl}$-uncastrated dorsolateral prostate, and 2 and 10 weeks after castration. Scale bar, 100 μm. **C,** Representative H&E images of *Pik3ca*$^{+/HR}$;*Pten*$^{fl/fl}$-uncastrated dorsolateral prostate and 2 weeks after castration. Scale bar, 100 μm; *n* = 5. **D,** Bar graph displaying total prostate weight normalized to body weight for *Pik3ca*$^{+/HR}$:*Pten*$^{fl/fl}$ mice 2 weeks after castration relative to age-matched/uncastrated controls (error bars, SEM; $P = 0.3394$, unpaired, two-tailed *t* test, *n* = 5). IHC quantitation for (**E**) PCNA and (**F**) CC3 in *Pik3ca*$^{+/HR}$, *Pten*$^{fl/fl}$, and *Pik3ca*$^{+/HR}$;*Pten*$^{fl/fl}$ dorsolateral prostate 2 weeks after castration compared with uncastrated/age-matched controls. Error bars, SEM; *, $P < 0.05$, one-way ANOVA with Tukey correction, *n* = 3. Mice were castrated when prostate carcinoma was prevalent; *Pik3ca*$^{+/HR}$ = 400 days old; *Pten*$^{fl/fl}$ = 200 days old; and *Pik3ca*$^{+/HR}$;*Pten*$^{fl/fl}$ = 100 days old.

Pik3ca Oncogenic Mutation and *Pten* Loss Synergize, Predisposing to *De Novo* CRPC

Next, we castrated *Pik3ca*$^{+/HR}$;*Pten*$^{fl/fl}$ mice at 100 days of age when invasive carcinoma was present, to test if *Pik3ca* mutation and *Pten* loss can also cooperate to promote CRPC growth. At 2 weeks after castration, castrated compound mutants phenocopied intact controls, and no appreciable difference in tumor burden was detected (Fig. 6C and D). These findings contrast the partial regression observed in the single mutants and indicate that *Pik3ca* oncogenic mutation and *Pten* homozygous deletion cooperate to promote *de novo* CRPC *in vivo*. In support, single mutants displayed a significant reduction in the percentage of PCNA-positive proliferative cells and elevated CC3-positive apoptotic cells 2 weeks after castration, which were unaltered in compound mutants (Fig. 6E and F; Supplementary Fig. S7A and S7B). These data indicate that *de novo* CRPC in *Pik3ca*$^{+/HR}$;*Pten*$^{fl/fl}$ mice is attributable to both the sustained level of proliferation and castration-induced apoptosis evasion. In accordance with *de novo* CRPC, IHC to detect AR also revealed that a noticeable proportion of *Pik3ca*$^{+/HR}$;*Pten*$^{fl/fl}$ prostate epithelial cells displayed AR activation (i.e., nuclear translocation) 2 weeks after castration, which was not apparent in single mutants at this early time point (Supplementary Fig. S6B). Of note, *Nkx3.1* and *Pbsn*, AR transcriptional target genes, are significantly reduced in *Pik3ca*$^{+/HR}$ prostate carcinomas relative to WT prostate, and levels were further diminished in *Pten*$^{fl/fl}$ and *Pik3ca*$^{+/HR}$;*Pten*$^{fl/fl}$ tumors (Supplementary Fig. S7C and S7D). These findings support previous work indicating that PI3K activation perturbs AR-mediated signaling (29) and indicate that *Pbsn* and *Nkx3.1* transcription is not likely to facilitate *de novo* CRPC in this setting.

The molecular mechanisms underpinning the emergence of CRPC are largely unknown. *Pten*-deleted CRPC acquisition has been previously associated with elevated AKT signaling, suggesting that further activation of the AKT cascade contributes to CRPC transition (9). In support, we observed a significant increase in the percentage of cells positive for mTORC1 signaling components pAKT (Thr308), pRPS6 (Ser235/236), and p4E-BP1 (Thr37/46) and the mTORC2 target pAKT (Ser473) in both the *Pik3ca*$^{+/HR}$ and *Pten*$^{fl/fl}$ models just 2 weeks after castration (Fig. 7A–D). Notably, phosphorylation of NDRG1 was not altered in either model after castration (Fig. 7E). Thus, *Pten*-deleted and *Pik3ca*-mutated prostate epithelial cells appear to hyperactivate AKT upon castration, which elevates mTORC1 signaling downstream targets to facilitate CRPC transition. Nevertheless, we do not exclude the possibility that additional molecular events may also contribute to CRPC transition in these models, including PTEN and/or AKT signal transduction independent of PI3K (2, 35).

Our analysis of *Pik3ca*$^{+/HR}$;*Pten*$^{fl/fl}$ prostate tumors before and after castration revealed that the high proportion of pAKT (Thr308)-, pRPS6 (Ser235/236)-, and pAKT (Ser473)-positive cells is maintained at a superactivated state, and that the percentage of p4E-BP1 (Thr37/46) and pNDRG1 (Thr346) cells is increased even further (Fig. 7A–E). Despite an increase in p4E-BP1 in *Pten*$^{fl/fl}$- and *Pik3ca*$^{+/HR}$;*Pten*$^{fl/fl}$-castrated tumors compared with *Pik3ca*$^{+/HR}$-castrated animals, p4E-BP1 was not significantly elevated in compound mutants compared with the *Pten*$^{fl/fl}$ model, signifying 4E-BP1 phosphorylation at Thr37/46 and subsequent inactivation are not likely to promote *de novo* CRPC formation. However, our findings suggest that NDRG1 inactivation may contribute to *de novo* CRPC. In addition to increased phosphorylation of NDRG1 after castration, androgen deprivation in *Pik3ca*$^{+/HR}$;*Pten*$^{fl/fl}$ mice also positively correlated with pNDRG1 nuclear localization (Fig. 7F). Nevertheless, the precise role of NDRG1 inactivation during *de novo* CRPC remains to be determined and warrants further investigation. Taken together, these results infer that a high threshold of AKT hyperactivation prior to castration, and/or NDRG1 inactivation, may prove to be useful biomarkers of intrinsic CRPC in the clinic.

To explore potential mechanisms underpinning the synergistic relationship between *Pik3ca* mutation and *Pten* deletion, and during castration-resistant disease formation, we performed a reverse-phase protein array (RPPA) on protein lysates isolated from *Pik3ca*$^{+/HR}$, *Pten*$^{fl/fl}$ and *Pik3ca*$^{+/HR}$;*Pten*$^{fl/fl}$ stage-matched uncastrated prostate carcinomas, and 2 weeks after castration (Fig. 7G; Supplementary Tables S6 and S7). RPPA data analysis revealed that *Pik3ca*-mutated and *Pten*-deleted prostate tumors display distinct RPPA profiles, supporting the contention that *Pik3ca* oncogenic mutation and *Pten* loss may mediate distinct signaling events to facilitate prostate cancer growth. For instance, compared with *Pik3ca*$^{+/HR}$ tumors, *Pten*$^{fl/fl}$ tumors displayed enhanced signal intensities for PI3K cascade phosphoproteins (e.g., pAKT Thr308, pAKT Ser473, pFOXO3A Ser318/321, pGSK-3β Ser9, and pNDRG1 Thr346), whereas tyrosine kinase–mediated (pEGFR Tyr1173, pSHP-2 Tyr542, pSRC family Tyr416) and MAPK (pERK1/2 Thr202/Tyr204) phosphoproteins were elevated in *Pik3ca*$^{+/HR}$ tumors (Fig. 7G; Supplementary Table S7). Interestingly, *Pik3ca*$^{+/HR}$ and *Pten*$^{fl/fl}$ prostate carcinomas did not display significant differences in RPPA signal intensities for the senescence markers p21 or p27 (Fig. 7G; Supplementary Table S7), suggesting that the observed phenotypic differences are not due to changes in senescence. A significant increase in p53 signal intensity was observed in *Pten*$^{fl/fl}$ tumors relative to *Pik3ca*$^{+/HR}$ tumors. As p21 and p27 are unaltered, these findings indicate that the observed changes in p53 are not regulating senescence, but may instead be mediating other cellular functions, such as apoptosis. This correlates with our observations in CC3 and phosphorylated p53 (Ser15; Fig. 7G; Supplementary Fig. S3B; Supplementary Table S7). RPPA results for pAKT Thr308 and pAKT Ser473 were confirmed by western blotting (Supplementary Fig. S7E).

RPPA profiles for uncastrated and castrated compound mutants were strikingly similar. Indeed, only four targets were significantly altered: pSHP2 (Tyr542) and pSRC family (Tyr416) signals were increased, and YAP and CK2α signals were decreased (Fig. 7G; Supplementary Table S7). This result contrasts single mutants that acquired CRPC and is consistent with the general lack of effect of castration on the prostate tumors in the double-mutant mice (Fig. 6C–F). However, it should be noted that the RPPA was not sensitive enough to detect elevated pNDRG1 (Thr346) in *Pik3ca*$^{+/HR}$;*Pten*$^{fl/fl}$ mutants after castration that was observed by IHC (Fig. 7E and F), presumably owing to tumor heterogeneity and/or stromal content, which may also be a contributing factor in

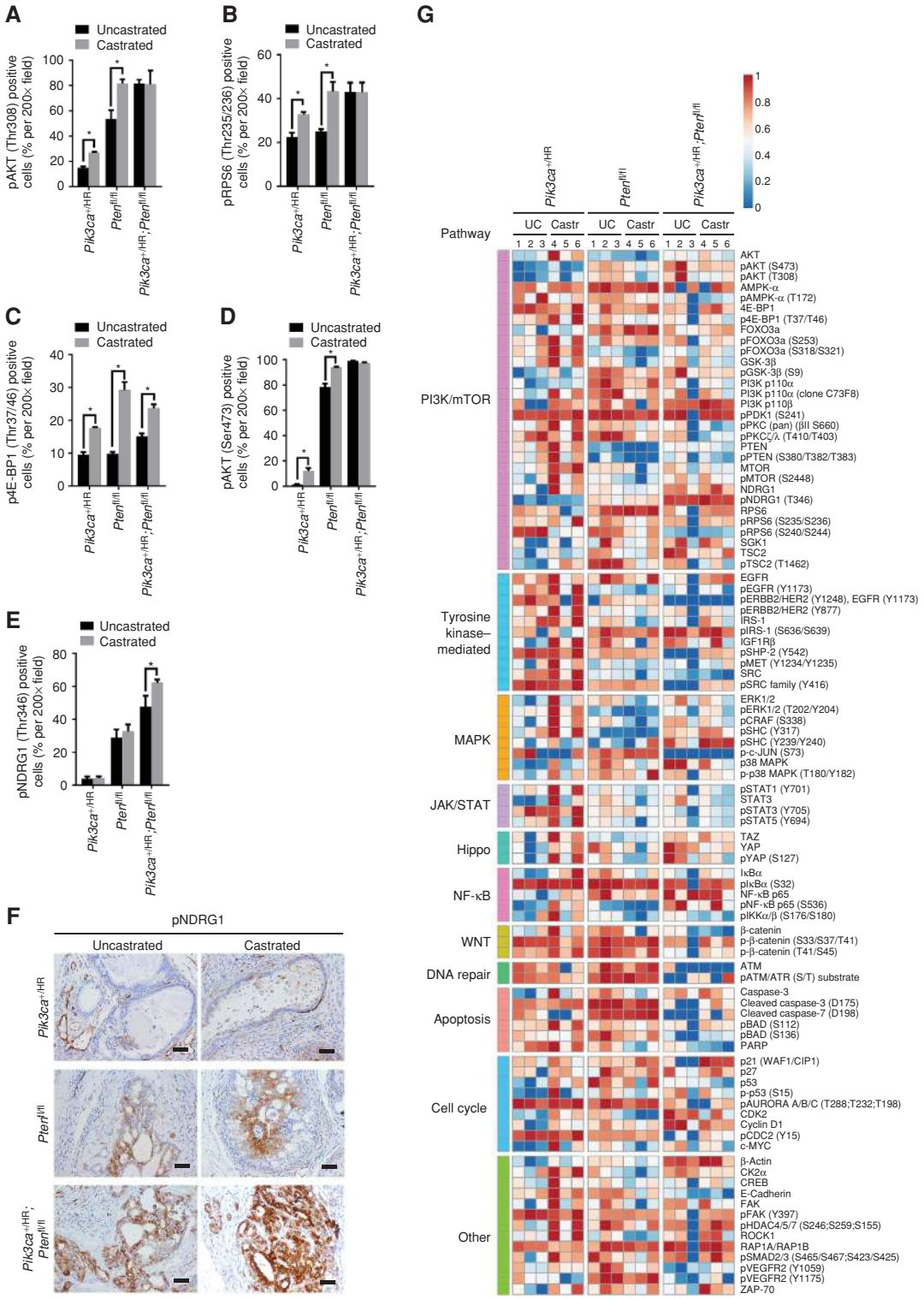

Figure 7. *De novo* CRPC in *Pik3ca*$^{+/HR}$;*Pten*$^{fl/fl}$ double transgenic animals correlates with NDRG1 inactivation. Quantitation of IHC to detect mTORC1 signaling components (**A**) pAKT Thr308, (**B**) pRPS6 Ser235/236, (**C**) p4E-BP1 Thr37/46, (**D**) pAKT Ser473, and (**E**) pNDRG1 Thr346 in *Pik3ca*$^{+/HR}$, *Pten*$^{fl/fl}$, and *Pik3ca*$^{+/HR}$;*Pten*$^{fl/fl}$ prostate tissue 2 weeks after castration compared with uncastrated, age-matched controls ($n = 3$; error bars, SEM; *, $P < 0.05$, one-way ANOVA with Tukey multiple comparison correction). **F,** Representative IHC images of pNDRG1 Thr346 in *Pik3ca*$^{+/HR}$, *Pten*$^{fl/fl}$, and *Pik3ca*$^{+/HR}$;*Pten*$^{fl/fl}$ prostate tissue 2 weeks after castration compared with uncastrated, age-matched controls. Scale bars, 50 μm; $n = 3$. **G,** RPPA analysis was performed on lysates from *Pik3ca*$^{+/HR}$, *Pten*$^{fl/fl}$, and *Pik3ca*$^{+/HR}$;*Pten*$^{fl/fl}$ prostate tissue 2 weeks after castration, and compared with uncastrated (UC), age-matched controls. Heat map represents Log_2-normalized and median-centered data (means of duplicates, $n = 3$ per cohort). Mice were castrated when prostate carcinoma was prevalent; *Pik3ca*$^{+/HR}$ = 400 days old; *Pten*$^{fl/fl}$ = 200 days old; and *Pik3ca*$^{+/HR}$;*Pten*$^{fl/fl}$ = 100 days old.

the lack of significant difference in other proteins as well. Nevertheless, distinct differences between the *Pik3ca*$^{+/HR}$ and *Pten*$^{fl/fl}$ models were detected after castration (Fig. 7G; Supplementary Table S7). For instance, *Pik3ca*-mutated tumors displayed a significant increase in IGF1Rβ and pNF-κB p65 (Ser 536) signal intensities after castration, which were not altered in *Pten*-deleted tumors after castration. In addition, castrated *Pik3ca*$^{+/HR}$ tumors displayed elevated JAK/STAT and MAPK signaling relative to castrated *Pten*$^{fl/fl}$ tumors. Taken together, our findings suggest that *Pik3ca* oncogenic mutation and *Pten* loss may mediate distinct signaling events to facilitate prostate cancer growth and resistance to castration.

DISCUSSION

We report that *PIK3CA* mutation/amplification positively correlates with poor prostate cancer patient prognosis and overall survival. Our findings are the first to demonstrate that the *PIK3CA*^{H1047R} oncogenic mutation is sufficient to cause invasive prostate cancer *in vivo* and that concomitant loss of *PTEN* and *PIK3CA* mutation, which frequently occurs in the clinic, can cooperate to accelerate prostate cancer growth in mice.

Our data support the hypothesis that different genetic drivers of the PI3K cascade are not functionally redundant, but instead drive prostate tumorigenesis via distinct signaling events. We show that relative to p110α-dependent *Pik3ca*$^{+/HR}$-induced prostate cancers, *Pten*$^{fl/fl}$ prostate tumors are p110α/β codependent and exhibit accelerated tumor formation and progression owing to AKT hyperactivation, elevated mTORC2, and RAC1–p110β signaling. The failure to induce robust AKT signaling in *Pik3ca*$^{+/HR}$ epithelium is probably attributable to the maintenance of PTEN tumor-suppressive function that reduces PIP_3 levels, AKT membrane recruitment, and subsequent activation of AKT, as previously reported (35). In corroboration, *Pten* loss has been shown to positively correlate with disease progression in mice, as *Pten* LOH is required for prostate cancer growth in *Pten* heterozygous prostate epithelium (9). We speculate that PTEN function is also likely to be conserved in transgenic mice expressing myristoylated/activated AKT or p110β in prostate epithelial cells, as only low-grade prostate epithelial neoplasia develops that does not progress to carcinoma with ageing (36, 37). Taken together, these observations suggest that additional mTORC2/RAC1/p110β-independent cooperative events are likely to facilitate malignant progression to an invasive state in *Pik3ca*$^{+/HR}$ mutants that express PTEN. Indeed, *PIK3CA* mutations have been shown to potentiate a PDK1–SGK3, AKT-independent signaling axis in various human cancer cell lines that express PTEN (35), and PDK1–SGK1, AKT-independent signaling has been shown to cause resistance to p110α inhibition by directly phosphorylating TSC2 to activate the mTORC1 pathway (38).

Guertin and colleagues have previously shown that *RICTOR*, a key regulatory component of mTORC2, is required for PC3 *PTEN*-null human prostate cancer cells to form tumor xenografts and that biallelic deletion of *Rictor* prevents prostate cancer formation driven by *Pten* loss in mice by reducing proliferation and AKT phosphorylation at Ser473 (39). We show that *Pten*$^{fl/fl}$ mice displayed early prostate tumor formation and accelerated progression relative to *Pik3ca*$^{+/HR}$ mutants, reflecting elevated mTORC2 signaling and subsequent AKT phosphorylation at Ser473 in the context of *Pten* loss. Thus, our findings support the notion that mTORC2 signaling plays a critical role during prostate tumorigenesis and progression, and strengthen the rationale for mTORC2-targeted therapy in *PTEN*-deleted prostate cancer.

The absence of pAKT Ser473 phosphorylation in *Pik3ca*$^{+/HR}$-mutant prostate cancer may be attributable to reduced PIP_3 levels and/or distinct AKT regulation in *Pten*-null and *Pik3ca*-mutant prostate cancers, as AKT phosphorylation is dependent on a plethora of AKT protein kinases and phosphatases (5). Of note, the mechanism of AKT regulation may also depend upon the type of *PIK3CA* mutation (i.e., helical vs. kinase) and tissue context, as several human cancer cell lines with *PIK3CA* kinase mutations have been shown to express high levels of pAKT Ser473 and Thr308 in the presence of PTEN (35). PTEN is also reported to play a broader AKT-independent tumor-suppressive role via protein- and lipid-phosphatase activities to mediate p53, cell-cycle arrest and integrin, insulin and focal adhesion kinase signaling, reviewed in ref. 40. Thus, developing our combined understanding of AKT regulation, p110 PI3K isoform signaling, and PTEN mode of action during prostate cancer is vital to determine optimal therapeutic approaches that inhibit the PI3K signaling network and subsequently prostate cancer growth and progression.

Although p110α and p110β isoforms have been shown to form mutually exclusive signaling complexes with RAS and RHO family (RAC1/CDC42) small GTPase protein superfamily members, respectively (22), the molecular mechanisms underpinning their different modes of action are poorly understood. This study provides additional data that underline a distinct role for the RAC1–p110β signaling axis in *Pten*-deleted prostate cancer, and raise the possibility that RAC inhibition may show therapeutic efficacy against *PTEN*-deleted prostate cancer in the clinic, as recently demonstrated for a *Pten*-null, p110β-dependent mouse model of myeloid neoplasia (41). By taking this approach, PI3K-independent functions of PTEN and AKT may be advantageously cotargeted, as RAC1 activation is mediated by PI3K-dependent (e.g., PREX1/TIAM/mTORC2) and PI3K-independent (e.g., SRC/p130CAS) signaling (25, 42).

We have generated a new clinically relevant transgenic mouse model of advanced prostate cancer driven by concomitant *Pik3ca* heterozygous oncogenic mutation and *Pten* homozygous deletion. We show that these two oncogenic drivers cooperate to promote rapid progression to invasive prostate cancer, characterized by the synergistic elevation of mTORC1/2 signaling, AKT superactivation, and increased *Pik3ca/b* mRNA transcript expression. These data provide direct evidence that *Pik3ca* mutation and *Pten* deletion coordinate independent oncogenic signaling events during prostate cancer, in corroboration with the distinct RPPA profiles observed. Furthermore, our findings emphasize that the coexistence of mutated *PIK3CA* and *PTEN* loss may prove to be an important prognostic indicator for rapid prostate cancer progression and *de novo* resistance to androgen deprivation therapy in the clinic.

Currently, the cause and consequence of upregulated *Pik3ca/b* transcription are poorly understood. Theoretically, increased *Pik3ca/b* gene expression could promote prostate cancer progression in *Pik3ca*$^{+/HR}$;*Pten*$^{fl/fl}$ mice by increasing p110α/β protein levels, and thus total PI3K activity, as *PIK3CA* amplification is thought to do in ovarian cancer cells

(43). FOXO3A, NF-κB, YB1, and p53 have been shown to promote *PIK3CA* transcription (reviewed in ref. 44); however, *PIK3CB* transcriptional regulators remain to be identified. Further investigation is needed to determine the underlying mechanism by which increased p110 catalytic activity and loss of PTEN phosphatase activity cooperate to upregulate *Pik3ca* and *Pik3cb* transcription, and to establish the functional significance of this observation.

Despite numerous phenotypic differences, we report that both *Pten*-null and *Pik3ca*$^{+/HR}$-driven prostate cancers are partially sensitive to androgen withdrawal and acquire CRPC in association with augmented PI3K signaling. These data signify that both p110α and p110β PI3K catalytic isoforms can induce PI3K signaling in response to androgen deprivation, supporting previous *in vitro* work in the PTEN-deficient human prostate cancer LNCaP cell line that showed PI3K signaling induced by an AR inhibitor is diminished by p110α or p110β inhibition (26). Because AKT hyperactivation and augmented mTORC1/2 are consistent features of intact *Pik3ca*$^{+/HR}$;*Pten*$^{fl/fl}$ prostate tumors, it is tempting to speculate that AKT hyperactivation may be a prerequisite for *de novo* CRPC in this setting. In addition, innate CRPC in *Pik3ca*$^{+/HR}$;*Pten*$^{fl/fl}$ compound mutants was associated with increased phosphorylation of the mTORC2–SGK substrate NDRG1 at Thr346, suggesting that NDRG1 inactivation may facilitate *de novo* CRPC. Significantly, NDRG1 has been shown to function as a metastasis suppressor in mouse xenograft models of prostate cancer by reducing *ATF3* transcription, and *NDRG1* mRNA downregulation correlates with Gleason score and worse prostate cancer survival (45). Stein and colleagues have also reported that NDRG1 is a p53 transcriptional target that is required for p53-mediated apoptosis (46). Given that *Pik3ca*$^{+/HR}$;*Pten*$^{fl/fl}$ prostate tumors evade castration-induced apoptosis and proliferation arrest, it will be important for future studies to determine if NDRG1 inactivation contributes to CRPC transition. However, because oncogenic PI3K/AKT signaling has been linked to increased genomic instability (47), we do not exclude the possibility that *Pik3ca*$^{+/HR}$;*Pten*$^{fl/fl}$ prostate tumors create an environment capable of inducing additional oncogenic mutations that promote CRPC formation.

It is becoming clear that approaches inhibiting multiple targets within the PI3K network, either simultaneously or sequentially, are necessary to enhance therapeutic efficacy. Thus, further characterization of p110α/β-mediated signaling, PI3K-independent PTEN tumor-suppressive functions, AKT-independent signaling, and AKT regulation is required to improve our understanding of how to target the PI3K network and identify mechanisms of therapeutic resistance to improve our management of prostate cancer in the clinic. Future work addressing how to personalize treatment for tumors driven by diverse PI3K genetic drivers is paramount and is likely to entail the coinhibition of PI3K-dependent and PI3K/AKT-independent signaling pathways.

METHODS

Experimental Animals

PBiCre transgenic mice that express *Cre* recombinase under the control of the Probasin promoter and *Pten*$^{fl/fl}$ mice have been described previously (21, 48). *Pik3ca*^{H1047R}-mutant mice were generated in-house (11). All mice were maintained on a pure FVB/NJ background. Mice were genotyped from DNA isolated from toe biopsies, as described previously (11, 49). Age-matched males were randomly assigned to uncastrated/castrated cohorts. Castration experiments involved the surgical removal of the testis and epididymis. Animal experiments followed the National Health and Medical Research Council (NHMRC) Australian Code of Practice for the Care and Use of Animals for Scientific Purposes and were approved by the Animal Experimentation Ethics Committee at Peter MacCallum Cancer Centre.

Tissue Isolation and Histology

Tissue was harvested and fixed for 16 to 24 hours in 10% neutral-buffered formaldehyde at 4°C before being paraffin embedded and sectioned at 4 μm. Sections were stained with hematoxylin/eosin for histologic analysis by a certified pathologist (P. Waring) blinded to genotype/treatment. Defining characteristics for prostate disease were based upon the pathologic classification of mouse prostate disease outlined in ref. 50.

Immunohistochemistry

Staining was carried out as described previously (49) on formalin-fixed, paraffin-embedded (FFPE) sections. Primary antibodies: Active RAC1–GTP 1:800 (#26903; NewEast Biosciences), AR 1:300 (#sc-816; Santa Cruz Biotechnology), PCNA 1:400 (#610665; BD Biosciences Pharmingen), and Cell Signaling Technology antibodies: Cleaved caspase-3 1:300 (#9664), pAKT (Ser473) 1:400 (#4060), pAKT (Thr308) 1:400 (#13038), pERK (Thr202/Tyr204) 1:200 (#4376), PTEN 1:300 (#9559), pRPS6 (Ser235/236) 1:400 (#2211), pNDRG1 (Thr346) 1:800 (#5482), and p4E-BP1 (Thr37/46) 1:200 (#2855). IHC scoring represents the mean percentage of positive cells counted from 8 to 10 images/mouse (×200 magnification, BX-51 Olympus microscope, $n = 3$/genotype).

PI3K Inhibitor Administration

Cohorts of male *Pik3ca*$^{+/HR}$ or *Pten*$^{fl/fl}$ mice were treated at 400 and 200 days old, respectively: A66 (p110α-specific inhibitor, 100 mg/kg, daily p.o.), TGX-221 (p110β-specific inhibitor, 30 mg/kg, daily p.o.), and BKM120 (pan-PI3K inhibitor, 40 mg/kg, daily p.o.). Inhibitors were dissolved in filter-sterilized 20% hydroxyproyl-beta-cyclodextrin (Sigma), sonicated for 10 minutes, and dosed immediately (4 weeks; 5 days on, 2 days off). No appreciable toxicity was observed (i.e., >20% weight loss). A66 and TGX-221 were generated in house by P.R. Shepherd (University of Auckland, New Zealand), and BKM120 was obtained from SYNkinase.

RNA Isolation and qRT-PCR Analysis

Total RNA extraction from mouse prostate tissue and qRT-PCR were performed according to standard methods described in the Supplementary Methods.

RNA In Situ Hybridization

FFPE mouse prostate tissue sections were probed using the RNAscope 2.5 high-definition red detection kit (#322350; Advanced Cell Diagnostics). Slides were counterstained with hematoxylin. Scoring represents the average number of RNA molecules per 50 cells/mouse (×400 magnification, BX-43 Olympus microscope, $n = 3$/genotype).

RPPA

Protein lysates were prepared from snap-frozen tissue homogenized in CLB1 buffer (Zeptosens, Bayer) and quantified using a Pierce Coomassie Plus (Bradford) Protein Assay Kit ($n = 3$/cohort). Using a Sciclone/Caliper ALH3000 liquid handling robot (Perkin Elmer), samples were serially diluted in 10% CLB1:90% CSBL1 buffer (Zeptosens, Bayer) and spotted onto ZeptoChips (Zeptosens) in duplicate

using a Nano-plotter-NP2.1 noncontact microarray system (GeSim). Chips were blocked under noncontact conditions for 1 hour with BB1 buffer (Zeptosens) and incubated with prevalidated primary antibodies (1:500, 20 hours) and Alexa Fluor 647 anti-rabbit secondary antibody (1:1,000, 4 hours; #Z-25308; Thermo Fisher Scientific). Chips were read on a Zeptosens instrument, and software version 3.1 was used to calculate the relative fluorescence intensity. All samples were normalized to the background values reported in the secondary antibody-only negative control. Pearson's correlation was calculated to confirm replicate pairs were adequately correlated (correlation coefficient >0.9). Data were Log_2-normalized, median centered and rescaled between 0 and 1 using the formula: $\frac{ab-\min(ab)}{\max(ab)-\min(ab)} \cdot ab$ represents a vector of antibody responses for a given sample. The RPPA heat map was generated in R using pheatmap. For details on western blotting validation, see the Supplementary Methods.

Analysis of Genomic Datasets

Analysis of *PIK3CA* gene mutation/amplification was performed on prostate cancer patient datasets with sequencing and copy-number alteration (CNA) data using the cBioPortal platform (14). The TCGA provisional dataset was downloaded from the TCGA data portal (https://tcga-data.nci.nih.gov/); *PIK3CA* segment mean Log R-Ratio ≥ 0.135. To minimize CNA noise, probe number was filtered to ≤10. Silent mutations were excluded.

Statistical Analysis

Prostate weight and IHC scoring were analyzed using a one-way ANOVA with Tukey correction or an unpaired *t* test (95% confidence interval) as indicated using GraphPad Prism_7.03 software. Kaplan–Meier plots were generated, and age-adjusted Cox proportional hazard regression ratio was calculated using R software. For RPPA, an unpaired two-tailed *t* test with Welch's correction was calculated using R software. $P < 0.05$ was considered statistically significant.

Disclosure of Potential Conflicts of Interest

No potential conflicts of interest were disclosed.

Authors' Contributions

Conception and design: H.B. Pearson, P.O. Humbert, W.A. Phillips
Development of methodology: H.B. Pearson, J. Li, A.A. Macpherson, K.J. Simpson
Acquisition of data (provided animals, acquired and managed patients, provided facilities, etc.): H.B. Pearson, V.S. Meniel, C.M. Fennell, P. Waring, K.G. Montgomery, R.J. Rebello, A.A. Macpherson, L. Furic, C. Cullinane, K.J. Simpson, T.J. Phesse, P.R. Shepherd, P.O. Humbert, W.A. Phillips
Analysis and interpretation of data (e.g., statistical analysis, biostatistics, computational analysis): H.B. Pearson, J. Li, K.J. Simpson, W.A. Phillips
Writing, review, and/or revision of the manuscript: H.B. Pearson, J. Li, C.M. Fennell, K.G. Montgomery, R.J. Rebello, L. Furic, C. Cullinane, R.W. Clarkson, M.J. Smalley, K.J. Simpson, T.J. Phesse, P.O. Humbert, O.J. Sansom, W.A. Phillips
Administrative, technical, or material support (i.e., reporting or organizing data, constructing databases): H.B. Pearson, J. Li, S. Koushyar, W.A. Phillips
Study supervision: H.B. Pearson, O.J. Sansom, W.A. Phillips

Acknowledgments

This work was generously supported by a Prostate Cancer Foundation of Australia concept grant (#CG 1611) and an NHMRC project grant (#1080491) awarded to W.A. Phillips, and a Peter MacCallum Cancer Foundation grant (#1520) awarded to H.B. Pearson. H.B. Pearson is supported by a Marie Skłodowska Curie Actions/Sêr Cymru II/ Horizons 2020 COFUND fellowship (#663830-CU-041). T.J. Phesse is supported by a Capital Medical University/Cardiff University Fellowship. L. Furic is supported by the Department of Health and Human Services acting through the Victorian Cancer Agency (MCRF16007). P.O. Humbert is supported by an NHMRC Senior Research Fellowship (#1079133). The Victorian Centre for Functional Genomics (VCFG) and the RPPA platform (K.J. Simpson) is funded by the Australian Cancer Research Foundation (ACRF), the Australian Phenomics Network (APN) through funding from the Australian Government's National Collaborative Research Infrastructure Strategy (NCRIS) program, the Peter MacCallum Cancer Foundation, and the University of Melbourne Collaborative Research Infrastructure Program. The authors wish to thank the animal, bioinformatics, VCFG-RPPA, microscopy, and histology core facilities at the Peter MacCallum Cancer Centre for supporting this project, and the histology departments at the Beatson Institute of Cancer Research and the European Cancer Stem Cell Research Centre. We also thank Nathan Crouch (VCFG-RPPA) for bioinformatics analysis of RPPA data, as well as Samantha McIntosh, Kerry Ardley, Susan Jackson, Lauren Dawes, Stephanie Le, Katherine Papastratos, and Qerime Mundrea at the Peter MacCallum Cancer Centre, Rachel Ridgway at the Beatson Institute for Cancer Research, and Derek Scarborough at The School of Biosciences, Cardiff University, for their technical assistance.

The costs of publication of this article were defrayed in part by the payment of page charges. This article must therefore be hereby marked *advertisement* in accordance with 18 U.S.C. Section 1734 solely to indicate this fact.

Received August 15, 2017; revised January 31, 2018; accepted March 16, 2018; published first March 26, 2018.

REFERENCES

1. Ferlay J, Soerjomataram I, Dikshit R, Eser S, Mathers C, Rebelo M, et al. Cancer incidence and mortality worldwide: sources, methods and major patterns in GLOBOCAN 2012. Int J Cancer 2015;136:E359–86.
2. Vanhaesebroeck B, Stephens L, Hawkins P. PI3K signalling: the path to discovery and understanding. Nat Rev Mol Cell Biol 2012;13:195–203.
3. Martini M, De Santis MC, Braccini L, Gulluni F, Hirsch E. PI3K/AKT signaling pathway and cancer: an updated review. Ann Med 2014;46:372–83.
4. Lemmon MA. Membrane recognition by phospholipid-binding domains. Nat Rev Mol Cell Biol 2008;9:99–111.
5. Chan CH, Jo U, Kohrman A, Rezaeian AH, Chou PC, Logothetis C, et al. Posttranslational regulation of Akt in human cancer. Cell Biosci 2014;4:59.
6. Garcia-Martinez JM, Alessi DR. mTOR complex 2 (mTORC2) controls hydrophobic motif phosphorylation and activation of serum- and glucocorticoid-induced protein kinase 1 (SGK1). Biochem J 2008;416:375–85.
7. Grasso CS, Wu YM, Robinson DR, Cao X, Dhanasekaran SM, Khan AP, et al. The mutational landscape of lethal castration-resistant prostate cancer. Nature 2012;487:239–43.
8. Taylor BS, Schultz N, Hieronymus H, Gopalan A, Xiao Y, Carver BS, et al. Integrative genomic profiling of human prostate cancer. Cancer Cell 2010;18:11–22.
9. Mulholland DJ, Tran LM, Li Y, Cai H, Morim A, Wang S, et al. Cell autonomous role of PTEN in regulating castration-resistant prostate cancer growth. Cancer Cell 2011;19:792–804.
10. Karakas B, Bachman KE, Park BH. Mutation of the PIK3CA oncogene in human cancers. Br J Cancer 2006;94:455–9.
11. Kinross KM, Montgomery KG, Kleinschmidt M, Waring P, Ivetac I, Tikoo A, et al. An activating Pik3ca mutation coupled with Pten loss is sufficient to initiate ovarian tumorigenesis in mice. J Clin Invest 2012;122:553–7.

12. Rudd ML, Price JC, Fogoros S, Godwin AK, Sgroi DC, Merino MJ, et al. A unique spectrum of somatic PIK3CA (p110α) mutations within primary endometrial carcinomas. Clin Cancer Res 2011;17:1331–40.
13. Forbes SA, Beare D, Gunasekaran P, Leung K, Bindal N, Boutselakis H, et al. COSMIC: exploring the world's knowledge of somatic mutations in human cancer. Nucleic Acids Res 2015;43:D805–11.
14. Gao J, Aksoy BA, Dogrusoz U, Dresdner G, Gross B, Sumer SO, et al. Integrative analysis of complex cancer genomics and clinical profiles using the cBioPortal. Sci Sign 2013;6:pl1.
15. Dogruluk T, Tsang YH, Espitia M, Chen F, Chen T, Chong Z, et al. Identification of variant-specific functions of PIK3CA by rapid phenotyping of rare mutations. Cancer Res 2015;75:5341–54.
16. Gymnopoulos M, Elsliger M-A, Vogt PK. Rare cancer-specific mutations in PIK3CA show gain of function. Proc Nat Acad Sci 2007;104:5569–74.
17. Abeshouse A, Ahn J, Akbani R, Ally A, Amin S, Andry Christopher D, et al. The molecular taxonomy of primary prostate cancer Cell 2015;163:1011–25.
18. Lin DI. Improved survival associated with somatic PIK3CA mutations in copy-number low endometrioid endometrial adenocarcinoma. Oncol Lett 2015;10:2743–8.
19. Yuan TL, Cantley LC. PI3K pathway alterations in cancer: variations on a theme. Oncogene 2008;27:5497–510.
20. Oda K, Stokoe D, Taketani Y, McCormick F. High frequency of coexistent mutations of PIK3CA and PTEN genes in endometrial carcinoma. Cancer Res 2005;65:10669–73.
21. Jin C, McKeehan K, Wang F. Transgenic mouse with high Cre recombinase activity in all prostate lobes, seminal vesicle, and ductus deferens. Prostate 2003;57:160–4.
22. Thorpe LM, Yuzugullu H, Zhao JJ. PI3K in cancer: divergent roles of isoforms, modes of activation and therapeutic targeting. Nat Rev Cancer 2015;15:7–24.
23. Rodriguez-Viciana P, Warne PH, Vanhaesebroeck B, Waterfield MD, Downward J. Activation of phosphoinositide 3-kinase by interaction with Ras and by point mutation. EMBO J 1996;15:2442–51.
24. Fritsch R, de Krijger I, Fritsch K, George R, Reason B, Kumar MS, et al. RAS and RHO families of GTPases directly regulate distinct phosphoinositide 3-kinase isoforms. Cell 2013;153:1050–63.
25. Zhang J, Gao X, Schmit F, Adelmant G, Eck MJ, Marto JA, et al. CRKL mediates p110β-dependent PI3K signaling in PTEN-deficient cancer cells. Cell Rep 2017;20:549–57.
26. Schwartz S, Wongvipat J, Trigwell CB, Hancox U, Carver BS, Rodrik-Outmezguine V, et al. Feedback suppression of PI3Kalpha signaling in PTEN-mutated tumors is relieved by selective inhibition of PI3K-beta. Cancer Cell 2015;27:109–22.
27. Wee S, Wiederschain D, Maira S-M, Loo A, Miller C, deBeaumont R, et al. PTEN-deficient cancers depend on PIK3CB. Proc Nat Acad Sci 2008;105:13057–62.
28. Jia S, Gao X, Lee SH, Maira SM, Wu X, Stack EC, et al. Opposing effects of androgen deprivation and targeted therapy on prostate cancer prevention. Cancer Discov 2013;3:44–51.
29. Carver BS, Chapinski C, Wongvipat J, Hieronymus H, Chen Y, Chandarlapaty S, et al. Reciprocal feedback regulation of PI3K and androgen receptor signaling in PTEN-deficient prostate cancer. Cancer Cell 2011;19:575–86.
30. Kang S, Denley A, Vanhaesebroeck B, Vogt PK. Oncogenic transformation induced by the p110beta, -gamma, and -delta isoforms of class I phosphoinositide 3-kinase. Proc Nat Acad Sci U S A 2006;103:1289–94.
31. Denley A, Kang S, Karst U, Vogt PK. Oncogenic signaling of class I PI3K isoforms. Oncogene 2008;27:2561–74.
32. Ferraldeschi R, Nava Rodrigues D, Riisnaes R, Miranda S, Figueiredo I, Rescigno P, et al. PTEN protein loss and clinical outcome from castration-resistant prostate cancer treated with abiraterone acetate. Eur Urol 2015;67:795–802.
33. Lunardi A, Ala U, Epping MT, Salmena L, Clohessy JG, Webster KA, et al. A co-clinical approach identifies mechanisms and potential therapies for androgen deprivation resistance in prostate cancer. Nat Genet 2013;45:747–55.
34. Zhang W, Zhu J, Efferson CL, Ware C, Tammam J, Angagaw M, et al. Inhibition of tumor growth progression by antiandrogens and mTOR inhibitor in a pten-deficient mouse model of prostate cancer. Cancer Res 2009;69:7466–72.
35. Vasudevan KM, Barbie DA, Davies MA, Rabinovsky R, McNear CJ, Kim JJ, et al. AKT-independent signaling downstream of oncogenic PIK3CA mutations in human cancer. Cancer Cell 2009;16:21–32.
36. Lee SH, Poulogiannis G, Pyne S, Jia S, Zou L, Signoretti S, et al. A constitutively activated form of the p110beta isoform of PI3-kinase induces prostatic intraepithelial neoplasia in mice. Proc Nat Acad Sci U S A 2010;107:11002–7.
37. Majumder PK, Yeh JJ, George DJ, Febbo PG, Kum J, Xue Q, et al. Prostate intraepithelial neoplasia induced by prostate restricted Akt activation: the MPAKT model. Proc Nat Acad Sci U S A 2003;100:7841–6.
38. Castel P, Ellis H, Bago R, Toska E, Razavi P, Carmona F J, et al. PDK1-SGK1 signaling sustains AKT-Independent mTORC1 activation and confers resistance to PI3Kα Inhibition. Cancer Cell 2016;30:229–42.
39. Guertin DA, Stevens DM, Saitoh M, Kinkel S, Crosby K, Sheen J-H, et al. mTOR Complex 2 is required for the development of prostate cancer induced by pten loss in mice. Cancer Cell 2009;15:148–59.
40. Blanco-Aparicio C, Renner O, Leal JF, Carnero A. PTEN, more than the AKT pathway. Carcinogenesis 2007;28:1379–86.
41. Yuzugullu H, Baitsch L, Von T, Steiner A, Tong H, Ni J, et al. A PI3K p110β–Rac signalling loop mediates Pten-loss-induced perturbation of haematopoiesis and leukaemogenesis. Nat Commun 2015;6:8501.
42. Ebi H, Costa C, Faber AC, Nishtala M, Kotani H, Juric D, et al. PI3K regulates MEK/ERK signaling in breast cancer via the Rac-GEF, P-Rex1. Proc Nat Acad Sci U S A 2013;110:21124–9.
43. Shayesteh L, Lu Y, Kuo W-L, Baldocchi R, Godfrey T, Collins C, et al. PIK3CA is implicated as an oncogene in ovarian cancer. Nat Genet 1999;21:99–102.
44. Thakur B, Ray P. p53 loses grip on PIK3CA expression leading to enhanced cell survival during platinum resistance. Mol Oncol 2016;10:1283–95.
45. Bandyopadhyay S, Wang Y, Zhan R, Pai SK, Watabe M, Iiizumi M, et al. The tumor metastasis suppressor gene Drg-1 down-regulates the expression of activating transcription factor 3 in prostate cancer. Cancer Res 2006;66:11983–90.
46. Stein S, Thomas EK, Herzog B, Westfall MD, Rocheleau JV, Jackson RS, et al. NDRG1 is necessary for p53-dependent apoptosis. J Biol Chem 2004;279:48930–40.
47. Xu N, Lao Y, Zhang Y, Gillespie DA. Akt: a double-edged sword in cell proliferation and genome stability. J Oncol 2012;2012:951724.
48. Lesche R, Groszer M, Gao J, Wang Y, Messing A, Sun H, et al. Cre/loxP-mediated inactivation of the murine Pten tumor suppressor gene. Genesis 2002;32:148–9.
49. Pearson HB, Perez-Mancera PA, Dow LE, Ryan A, Tennstedt P, Bogani D, et al. SCRIB expression is deregulated in human prostate cancer, and its deficiency in mice promotes prostate neoplasia. J Clin Invest 2011;121:4257–67.
50. Shappell SB, Thomas GV, Roberts RL, Herbert R, Ittmann MM, Rubin MA, et al. Prostate pathology of genetically engineered mice: definitions and classification. The consensus report from the Bar Harbor meeting of the Mouse Models of Human Cancer Consortium Prostate Pathology Committee. Cancer Res 2004;64:2270–305.